Annette Bretin

Elastic Properties of the Human Femur

Local Anisotropic Material Laws for Patient-Specific Modelling

Research Series of the Clinic for Orthopaedics and Trauma Surgery University of Lübeck – Volume 2

Infinite Science Publishing

LÜBECK UNIVERSITY PRESS

Imprint of Infinite Science GmbH,
Technikzentrum | MFC 1
Maria-Goeppert-Straße 1
23562 Lübeck, Germany

Cover Design and Illustration: Infinite Science Publishing and Annette Bretin
Editorial and Copy Editing: University of Lübeck, Clinic for Orthopaedics and Trauma Surgery

Publisher: Infinite Science GmbH, Lübeck, www.infinite-science.de
Printed in Germany, BoD, Norderstedt

ISBN 978-3-945954-55-3

Bibliografische Information der Deutschen Nationalbibliothek:
Die Deutsche Nationalbibliothek verzeichnet diese Publikation in der Deutschen Nationalbibliografie; detaillierte bibliografische Daten sind im Internet über http://dnb.d-nb.de abrufbar.

ZUSAMMENFASSUNG

Die Materialzuweisung ist ein diffiziler Aspekt in der Generierung patienten-spezifischer Computermodelle von Knochen. Ein Ansatz basiert auf der Dichteabhängigkeit elastischer Eigenschaften des Knochens, jedoch reflektieren bestehende Gesetze nur unzureichend dessen Anisotropie und Inhomogenität. Primäres Ziel dieser Arbeit war die Bestimmung von dichtebasierten, orthotropen Materialgesetzen in homogenisierten, lokalen Zonen des Femurs, um die Materialzuweisung in Finite-Elemente-Modellen zu präzisieren.

7 humane Femora verstorbener Personen wurden in 14 lokale Zonen eingeteilt. Kortikale Proben wurden entnommen und in Druck- und Torsionsversuchen getestet. Videoextensometrie basierend auf digitaler Bildkorrelation wurde verwendet, um 9 orthotrope Elastizitätskonstanten zu bestimmen. Spongiöse Proben wurden virtuell extrahiert. Die Elastizitätskonstanten wurden hier mittels Finite-Elemente-Methode auf Mikroebene prognostiziert. Die ermittelten Konstanten wurden mit der radiologischen Knochenmineraldichte der jeweiligen Probe korreliert, die mithilfe quantitativer Computertomografie bestimmt wurde. Für spongiöse Proben wurde jede Konstante zudem mit einer aus dem Volumenanteil des Knochens bestimmten Dichte korreliert.

Zusammengefasste Resultate der Elastizitäts- und Schubmoduln über alle Zonen der Kortikalis zeigten signifikante Korrelationen zur Dichte. Die kortikalen Poissonzahlen wiesen hingegen keinerlei Korrelationen zur Dichte auf. In den spezifischen Zonen der Kortikalis konnten solche Korrelationen lediglich für longitudinale Elastizitätsmoduln in der ventralen, medialen und dorsalen Diaphyse, sowie für einen Schubmodul in der ventralen Diaphyse nachgewiesen werden. Gründe hierfür wurden der geringen Anzahl an kortikalen Proben, sowie Ungenauigkeiten in der Bestimmung der Knochenmineraldichte zugeschrieben. Dagegen wiesen alle orthotropen Elastizitätsmoduln und Schubmoduln der spongiösen Zonen eine signifikante Korrelation zur Dichte auf, mit Ausnahme eines Schubmoduls im Zugbündel des Femurhalses, in dem nur wenige Proben zur Verfügung standen. Die statistische Aussagekraft der Gesetze war im Allgemeinen höher, wenn die Knochenmineraldichte eingesetzt wurde, die mittels Volumenanteil des Knochens bestimmt wurde. Orthotrope Poissonzahlen zeigten gelegentlich signifikante Korrelationen zur Dichte, was auf eine Abhängigkeit zu weiteren Faktoren hinweist, wie die Geometrie der trabekulären Strukturen.

ABSTRACT

The assignment of material properties is a challenging aspect of patient-specific modelling of bone. One approach is the material assignment based on the correlation of elastic material properties to bone mineral density. Yet, available material laws do not sufficiently reflect the anisotropy and the inhomogeneity of bone. The primary goal of this doctoral thesis was the establishment of orthotropic elasticity-density relationships in homogenized, local femoral zones, to improve the assignment of material properties in finite element models.

7 human cadaveric femora were subdivided into 14 local zones. Cortical bone samples were extracted and tested in compression and torsion tests. Videoextensometry based on digital image correlation was used to determine all 9 orthotropic constants. Cancellous samples were virtually extracted and the elastic properties were predicted by micro finite element analysis. All determined constants were correlated to the radiological bone mineral density of each sample, which was determined by quantitative computed tomography. In case of cancellous bone, each constant was additionally correlated to bone mineral density, determined from the bone volume fraction of each sample.

Pooled results over all zones yielded significant correlations to bone mineral density for all Young's and shear moduli, but the cortical Poisson's ratios did not result in significant correlations to density. In the specific zones of cortical bone, only longitudinal Young's moduli in the anterior, medial and posterior diaphysis and one shear modulus in the anterior diaphysis revealed significant correlations to density. The reasons were attributed to the low amount of investigated cortical samples and inaccuracies in the determination of bone mineral density. In contrast, significant correlations to bone mineral density were found for all orthotropic Young's and shear moduli in all cancellous zones, except for one shear modulus in the tensile bundle of the femoral neck, in which the number of investigated samples was low. The statistical power of established laws was in general higher when the bone density derived from bone volume fraction was used. Orthotropic Poisson's ratios did occasionally reveal significant correlations to density, suggesting that the material behaviour is also dependent on other factors, such as the geometry of trabecular structures.

CONTENTS

1 INTRODUCTION

1.1 MOTIVATION

1.1.1 PATIENT-SPECIFIC MODELLING

During the last decade researchers and clinicians started to evince high interest in patient-specific modelling (PSM). The generation and use of realistic computer models enable the prediction of clinical outcomes by numerical simulations and thereby, enhance evidence-based treatment of patients. They provide the possibility to optimize diagnosis as well as individual therapies or surgical interventions (1). Meanwhile, diverse tissues and organs have been investigated using PSM, covering huge research fields and clinical issues. Blood vessels for instance have been examined regarding their mechanics, the prediction of aneurysms and the inspection of blood flow (1-3). Another preferred field of application is the heart including investigations on electrophysiological and electromechanical processes, valve mechanics, ventricular fluid flow as well as hemodynamics (1, 4-8). With respect to the brain, the impact of deep brain stimulation, surgical procedures or intracranial pressure dynamics in traumatic brain injuries have been investigated (1, 9). Even in oncology, PSM has been used to examine the individual mechanics of tumour growth or to optimize cancer treatment such as radiation therapy, chemotherapy or laser treatment (1, 10, 11). In orthodontics, PSM of the mandible is capable to predict individual tooth movement and the influence of molar loss on the mechanical condition in the periodontium (1). Simulation of muscles can be beneficial in the treatment of deep tissue injuries, in the optimization of prosthetic design or to develop new medical devices (1, 12). On the basis of kinematic and kinetic pre-treatment data, multibody dynamical simulations have also been used for the prediction of individual post-treatment walking patterns being affected by the particularly applied interventions (1, 13).

Similar investigations have been performed for bone. Vertebrae for instance have been examined to predict the patient-specific progression of scoliosis and to optimize scoliosis corrective surgery (1). PSM can also be beneficial in the treatment of osteoarthritis or to predict the impact of total hip arthroplasty (1).

Researchers even seek to perform patient-specific *in vivo* bone remodelling simulations to predict individual load-adaptive bone formation (14, 15), which may positively affect post-operative treatment such as physiotherapeutic therapies. Patient-specific bone simulation can further be beneficial for the prediction of fracture risk and to improve surgical procedures by pre- or intraoperative planning of implant placement (16, 17). One of the major motives for the conduction of this study was the potential of prosthetic design optimization using PSM. Size and shape of implants can be customized to meet the demands of the individual mechanical condition, which might reduce the necessity of revision surgeries and thereby, improve the clinical outcome and physical state of patients while reducing costs for the health care system.

1.1.2. PATIENT-SPECIFIC MODELLING OF BONE

Mechanical bone simulation is based on finite element analysis (FEA). Involving Hooke's law, this method allows the calculation of strains, stresses and displacements of linearly-elastically loaded objects of arbitrary geometry by subdividing the entire object into small elements (finite elements). The physical description of the discretized primitive structures (i.e. tetrahedrons or hexahedrons) can be approximated by applying linear or higher order mathematical functions to predict the solution. The functions of all single elements can be combined resulting in a system of partial differential equations. From the solution of each equation the mechanical behaviour of the entire object can be concluded (1, 18).

Although this approach seems to be trivial, a large amount of *a priori* knowledge is necessary to generate an ideal patient-specific model of bone. The subject-specific osseous anatomy must be known, which can be derived by imaging modalities such as computed tomography (CT) or magnetic resonance imaging (MRI) (16). From the image data, osseous structures can be segmented and stored as surface or volume data that describe the subject-specific osseous anatomy. This information is in general used for discretization as the finite element mesh is generated according to the segmented structures. For the application of individual boundary conditions, patient-specific kinetic data needs to be provided to predict essential load directions during the individual dynamic movement. These kinetic data can be derived from patient-specific motion analysis. The specific

kinematic data must be obtained likewise to describe the magnitude of muscle and joint reaction forces, which can be acquired from patient-specific muscle simulation. Kinematic and kinetic data have also been successfully derived from *in vivo* measurements of shoulder, hip and knee implants via telemetric data transmission (19-24), but this approach is restricted to patients with joint replacements. It may provide approximated generalized information on mechanical conditions within human joints, yet it might not be valid for all patients.

Another essential *a priori* knowledge is the subject-specific material properties within the bone, which have to be assigned to the finite element model. Up to now, this topic is extremely challenging, since bone involves complex material characteristics. It is inhomogeneous as the structure and thereby its properties are unevenly distributed. In addition, it is anisotropic with material properties depending on direction. Bone can acceptably be assumed to show orthotropic behaviour (25-29). An orthotropic material is characterized by three orthogonal planes of symmetry (see chapter 2.2.2). This direction dependency can generally be expressed in Cartesian coordinates in the finite element model, but bone is curvilinear orthotropic, i.e. the directionality of the coordinate system varies over the osseous structure according to the local stress conditions. Additionally, the degree of anisotropy changes across each individually regarded bone as well, leading to the following conclusion: the material properties are ideally assigned to each finite element according to the local principal stress directions, the degree of anisotropy as well as the local magnitude of elastic properties. Such an approach is numerically demanding and requires a very precise formulation of patient-specific bone stiffness.

Poelert et al. (2013) propose, that the accuracy, reliability and practicability of patient-specific bone modelling needs to be ensured before it can be established in clinical routine (16). In this context, researchers still face a lot of obstacles. The segmentation methods as well as the mesh generation strategies for instance influence the results of FEA (30, 31). Another challenging fact is the low resolution in common clinical imaging excluding micro finite element analysis (μFEA), the gold standard of numerical analysis for PSM. Low resolution image data influence the geometric description of the specific bone, which might lead to error propagation. The thickness of the femoral cortex for instance is highly reduced in

the femoral neck region. The resulting thin layer cannot be appropriately depicted in clinical CT or MRI images (32, 33). Pahr et al. (2009) applied a thickness correction algorithm to include the thin cortex layer into the finite element model correctly, but the method was restricted to high-resolution CT or MRI (33) with a resolution beyond those of common clinical scanners. PSM might benefit from applying such kind of correction algorithms to low resolution images based on *a priori* population knowledge. Another problem is the bone architecture, which cannot be depicted in low-resolution image data. To overcome this problem patient-specific finite element models of bone have been commonly homogenized, although researchers found that a precise representation of cortex and trabecular architecture influences the prediction of stiffness and strength (34). Homogenized models are based on the assumption that bone is a continuum, disregarding the differentiation between bone and marrow.

To account for the inhomogeneity of bone, density-based material assignment has been applied in numerous studies using homogenized finite element models (17, 30, 32, 35-43). Elastic properties are inhomogeneously assigned to the finite element mesh according to the local bone mineral density (BMD) derived from the grey value of the involved image data. The described method includes two assumptions. First, the image intensity within each voxel correlates with the density of bone. Secondly, bone density is assumed to correlate with its elastic properties as described by the various published material laws. The application of density-based inhomogeneous material assignment to finite element models was proven to be more accurate than homogeneous material mapping (32), but there are still several inconsistencies.

For the establishment of material laws, researchers did not only use different measurement techniques and test protocols but most notably, they extracted samples from different anatomical locations. This might be one of the major reasons for the variety of material laws in literature, since bone formation is affected by the specific stress condition (44-46) resulting in an altered composition and architecture at distinct anatomical locations. Such alterations are likely to affect the elasticity-density relationships as well. Morgan et al. (2003) found significantly different elastic material laws at distinct anatomical sites (47).

Cortical and trabecular bone is commonly distinguished in density-based material mapping. Each bone type is assumed to relate to a distinct elasticity-density law with respect to their structural difference. The transition between cortical and trabecular structures can cause problems in low resolution images, since partial volume effects affect the grayscale intensity within the image. To overcome this problem, correction algorithms can be applied (17, 48).

Some established material laws in literature involve different formulations of density, such as ash or apparent bone density (49). This further increases the variety of existing material laws. For the use of clinical image data, a density indication such as radiological BMD would be reasonable.

1.1.3. STATE-OF-THE-ART BONE MODELLING

Researchers initially applied inhomogeneous but isotropic material behaviour, i.e. only one density-based material law was applied to all directions (32, 39). This simplification was assumed to be attributable to the lack of comprehensive empirical knowledge about the orthotropic material behaviour (27). The method was enhanced by orthotropic material mapping but first the change in directionality was not considered, since only one Cartesian coordinate system was used for the entire bone (37). Yang et al. (2010) described the comparison of an inhomogeneous isotropic and orthotropic model, including two basic directionalities of the femoral neck and stem. They included different load cases into their study and found differences in Von Mises stress of up to 13% as well as differences in local displacement of up to 15% (50). Baca et al. (2008) generated a global, as well as local finite element models including orthotropic material laws (51). 30 different orthotropic orientations were considered that were derived from the internal structure of the bone. They found differences in relative deformations of up to 7.4% for their global model and of up to 64.5% for the local models in comparison to the respective inhomogeneous isotropic models, emphasizing the need for a more precise material assignment in PSM of bone. None of the mentioned researchers considered a changing degree of orthotropy and the formulations of density-dependent elastic constants were partially based on assumptions (37, 50, 51). Conclusively, the error in simulated displacements might be even more significant.

Different strategies evolved recently to increase the reliability of patient-specific bone modelling from clinical imaging, which involve a more accurate orthotropic representation of the patient-specific bone. Kober et al. (2006) constructed orthotropic trajectories in the human mandible from CT scans, indicating the local orientation of material properties at each position. The construction of these trajectories were based on the anatomical shape of the mandible as well as on structural equivalents depicted by similar image intensities (52). Hellmich et al. (2008) mapped voxel-specific orthotropic stiffness tensors on their finite element model of the human mandible (53). Both approaches were used for finite element simulations resulting in elastic strains, which differed from those of isotropic models (52, 53).

Other authors used image processing techniques such as gradient structure tensors and Sobel structure tensors to conclude the orientation and degree of anisotropy from low resolution images. Such approaches turned out to be only suitable for bones with a high degree of anisotropy (54, 55).

The solution of FEA has also been used to derive the orthotropy of bone from clinical CT. According to the loading condition trabecular orientation can be reversely constructed from the resulting stresses, since the stress state is assumed to influence bone remodelling (see chapter 2.1.3). The procedure works well for the orientation of the first principal stress direction. However, second or third principal direction as well as degree of orthotropy was either not determined or yielded poor results (56, 57). Trabelsi & Yosibash (2011) tried a similar approach on the proximal femur involving the resulting strain instead of stress conditions, since the elastic strain present in the femur is known to be almost independent from resulting hip forces (58). They also applied a surface-based approach to determine trajectories and compared both methods. The orientation of the resulting trajectories differed but they had no significant effect on finite element results. Hence, the precision of each approach remains unclear.

In the nineties, Zysset and Curnier (1995) developed a powerful theoretical model describing the mathematical relation between material elasticity and trabecular architecture (59-61), which can be calibrated by respective material characteristics such as the volume fraction, fabric tensor and homogenized elastic properties (61-63). Using such method, anisotropic characteristics can be approximated from

trabecular fabric, which needs to be derived from high-resolution imaging. These considerations have been recently used as *a priori* knowledge for the generation of homogenized patient-specific finite element models. Marangalou et al. (2013) for instance generated a homogenized patient-specific finite element model based on the Zysset Curnier model. Their patient-specific anisotropic material properties were predicted based on a similar bone taken from a comprehensive database of cadaveric samples, which were scanned with high resolution. Detailed material properties were derived and mapped to the homogenized patient-specific model by mesh morphing. Compared to the gold-standard (i.e. μFEA) the error in stiffness prediction remained below 5 %, whereas a respective isotropic model underestimated bone stiffness by 26.3 % (29). Taghizadeh et al. (2016) successfully mapped one anisotropic model of the femur derived from high-resolution scans to a patient-specific proximal femur by image registration. A finite element model was generated by mapping the fabric tensor to each element of the mesh and material properties were assigned according to the Zysset Curnier model. Subsequent finite element simulations resulted in displacement errors being reduced from 7.3 % to 2.5 % compared to an isotropic model (64). Another approach for the orthotropic description is based on anisotropic statistical models, i.e. statistically averaged trabecular fabric from a database. Lekadir et al. (2015) established a regression model of femoral trabecular fabric, resulting in a precise description of the orthotropic orientation and the degree of anisotropy (65). Recently, statistical models of shape, bone volume fraction (BV/TV) and fabric were combined to examine the correlation among these bone parameters. Such linkage would enable a prediction of fabric from clinical CT scans, but the correlations found between the three parameters were weak (66). Yet, homogenized finite element simulations confirmed the suitability of the average anisotropic statistical model (66). One main disadvantage of using statistical models for anisotropic material assignment is the database necessary to give *a priori* information on fabric involving a corresponding number of high-resolution image data.

An entirely different statistical approach to assign orthotropic material properties is to establish more precise formulations of elasticity-density laws from specified regions of different femora, which is the topic of this doctoral thesis. Up to now, elasticity-density-based material mapping of bone lacks a comprehensive

formulation of local anisotropy. This doctoral thesis addresses the behavioural description of all nine orthotropic elastic constants and involves information about the principal orthotropic orientations within the cluster. The approach eliminates the need for databases. It might also keep the computational effort of numerical models on a lower level depending on the interpolation method for material properties in the transition of zones. Zone-specific elasticity-density laws can further be used to generate simple finite element models for local investigations.

1.2 SPECIFIC AIMS OF THE STUDY

The primary goal of this study was to correlate anisotropic elastic material properties to BMD in homogenized local femoral zones. With the resulting laws, material properties can be assigned to local or global patient-specific finite element models of the human femur. Specifically, the following aims were defined for this doctoral thesis:

I. The femur had to be divided into local zones of similar mechanical functions and structural conditions that can be purposefully clustered. Stress conditions within the femur as well as structural organization and local functions of femoral sections were examined for this purpose.

II. The radiological BMD of bone samples needed to be determined for cortical and cancellous bone. In order to evaluate the suitability of the method for common clinical practice the resulting error in the determination of BMD was investigated.

III. To link the BMD to the measured elastic properties methods enabling a defined extraction of test samples had to be developed for both bone types to ensure the segmentation of the identical samples from their respective CT scan.

IV. Appropriate methods capable of detecting even marginal elastic strains needed to be developed and validated, in order to determine mechanical properties of small specimens for cortical bone and cancellous bone.

V. All nine elastic constants had to be determined and correlated with the BMD of the corresponding sample. Resulting regressions were calculated and statistically examined. Their applicability was evaluated and material laws of different zones were compared to evaluate the necessity of the precise material law assignment.

VI. Vectors had to be provided for each defined cancellous zone, which describe the average three-dimensional orthotropic orientation of the cluster within a reference coordinate system. Such vectors represent approximated local orientations of invisible trabecular architecture in low-resolution image data associated with the herein determined orthotropic elasticity-density laws.

1.3 STRUCTURAL OUTLINE

Chapter 2 provides the scientific background needed to comprehend the applied methods as well as the result and discussion section to the full extent for readers unfamiliar with the topic. Chapter 3 addresses the description of all necessary approaches for the determination of density-based material laws including the accomplishment of aim I-IV. It further contains the description of methods used to evaluate respective approaches. Chapter 4 illustrates all results including the validation of test methods, the elasticity-density relationships and directionality of orthotropy within the specific cancellous zones as requested by aim V and VI. Chapter 5 provides a comprehensive discussion of the methods and the results, with focus on the specific aims. The discussion is followed by conclusions being drawn in chapter 6.

2 SCIENTIFIC BACKGROUND

In this chapter background information is provided for the interested reader or for readers unfamiliar with the topic. Mechanical fundamentals of bone are addressed in the first subchapter, providing an introductory step into the topic. A basic overview on elastomechanics is provided in the second subchapter being of substantial importance to understand the principals of this work. Information on diverse bone measurements will complement the scientific background to fully understand methodological strategies.

2.1 HUMAN FEMORAL BONE IN THE MECHANICAL CONTEXT

Femoral mechanical properties rely on compositional and morphological aspects, which are inevitably linked to diverse influences such as the individual mechanical conditions, age or diseases. Fundamentals of femoral bone composition of healthy human adults as well as on intrinsic and extrinsic conditions affecting its mechanical characteristics are provided first. As a result, this chapter shall lead to a comprehensive understanding of the various mechanical properties in literature, determined from individually or locally diverse bone specimens. The second subchapter addresses the organizational structure of the femur on the macro level and provides general information on the mechanical condition. It serves as preparation for the division into femoral zones in chapter 3.3. The third subchapter focuses on the anisotropic adaption of trabecular fabric and its mathematical integration to fully comprehend the morphological examination of cancellous bone specimens explained in chapter 2.3.2 and 3.7.1.

2.1.1. COMPOSITIONAL AND MECHANICAL FUNDAMENTALS OF FEMORAL BONE TISSUE

The human femur is a long bone located in the thigh. From a clinical point of view, it is one of the most relevant bones. Hip fractures in the proximal femur for instance are frequent causes for surgical interventions with high mortality risks (67). The femur is part of the hip and the knee joint, which are both prone to be replaced due to osteoarthritis in elderly people (68). There are plenty of other reasons for femoral surgeries such as fractures of the femoral shaft or osseous sarcomas. Since it may be useful for a wide range of surgical treatments, patient-specific finite element analyses of the femur are of high importance.

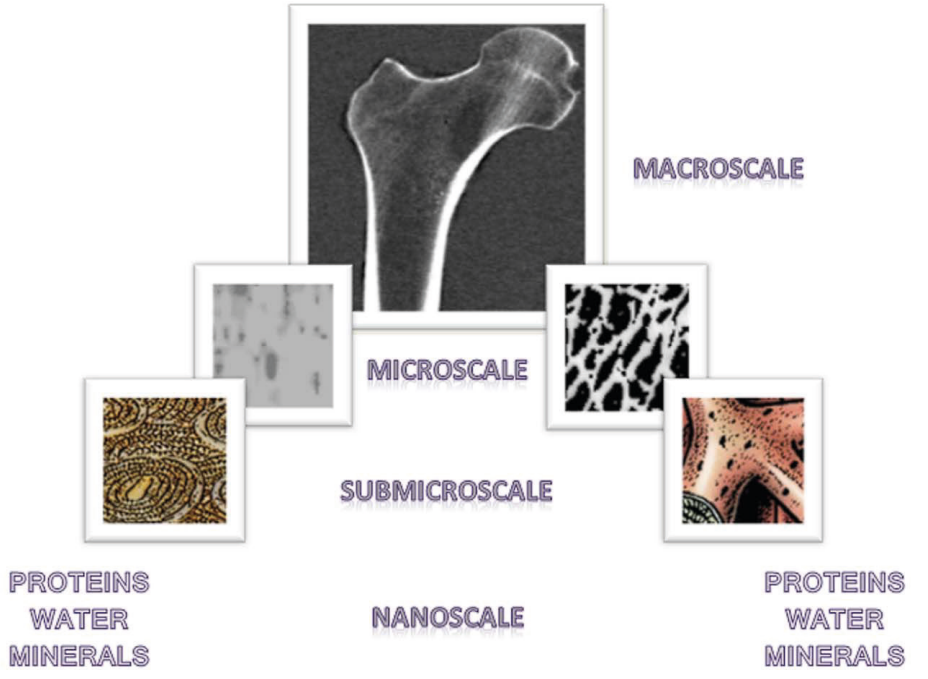

FIGURE 2.1: SCHEMATIC DRAWING OF BONE FROM MACRO- TO NANOSCALE.

In general, bone is a viscoelastic material whose composition is affected by activity, age and diseases (69). It features a compositional structure on different scales (69). To understand the mechanical aspects of the human femur on the macro scale, a closer observation of bone tissue from micro- to nanoscale is required. The different levels and compositions are illustrated in Figure 2.1 and outlined subsequently.

On the molecular level, half of the bone matrix volume generally consists of water and organic material such as collagen fibrils as well as noncollagenous proteins. The other half consists of calcium phosphate crystals such as hydroxyapatite (69, 70). The bone mineral constitutes 2/3 of the bone's weight (69), indicating a higher density compared to the remaining components. It is an essential component in terms of mechanical behaviour, as it stiffens the before mentioned organic material by impregnating and surrounding the collagen fibrils (70). The assessment of BMD, i.e. the magnitude of mineralization in the inhomogeneously distributed bone tissue, plays a major role in clinical practice as it is used as an indicator for the fracture risk (71). It has also been widely used to predict the elastic behaviour as

outlined in chapter 1. Various mechanical properties do not only depend on the amount of inorganic bone minerals, but also on the amount of water and organic material as well as on the linkage between collagen and crystals or on the conditions of collagen fibrils (69). Molecules of collagen fibrils are for instance intra- and intermolecular cross-linked, which is known to increase tensile strength (69). Noncollagenous proteins are assumed to influence calcification (69, 70) as well as bone reconstruction or the binding between collagen and minerals (70). Consequently, there may be further molecular influence on the mechanical properties of bone.

In general, different cell types are present in bone, all fulfilling a specific task. Bone lining cells for instance built the periosteum and endosteum. They cover the bone surface and the blood vessels, regulating the transition of ions (70). Further cells are osteoblasts, which are bone-forming cells (70). They are also assumed to regulate the mineralization of the bone matrix (72). Osteoclasts are responsible for the destruction of old bone (70, 72). Both, osteoclasts and osteoblasts, play a major role in bone remodelling as outlined in chapter 2.1.3. Osteocytes are the cells within the bone, being responsible for its maintenance and believed to be the main mechanosensors (72). They are surrounded by the bone matrix (45, 70, 72) and connected by canaliculi, which enable the sharing of nutrients between different osteocytes (72). Due to the various tasks, the mentioned cell types do also affect the mechanical behaviour of bone, especially those, who are responsible for remodelling and mineralization.

On the macro scale, the human femur can be divided into cortical bone, also called compact bone and cancellous bone, also referred to as trabecular or spongious bone. Cancellous bone is metabolically more active and more responsive to mechanical variations compared to cortical bone (69). Considering load bearing aspects, cortical bone provides rigidity while the porous cancellous structure absorbs energy and distributes forces (69). The bone marrow, which can be found in the medullary cavity as well as in the intertrabecular spaces (45), has no significant impact on bone mechanics (70).

The cortical tissue forms the cortex of the femoral bone below the periosteum and the articular cartilage. Its structure is solid accommodating only some small cavities (70). Although it seems to be a homogeneous material at first sight, its

inhomogeneity becomes evident by measuring its BMD, which is unevenly distributed. On the micro and sub-microscale, cortical bone consists of longitudinally running osteons. They contain concentric lamellae including a cavity for blood vessels and nerves in the centre (45, 70, 73, 74), supplying oxygen and nutrients to the osteocytes and enabling nerval stimulation. Such cavities are called Haversian canals (74). Perpendicular to these canals additional cavities run between the outer and inner bone, called Volkmann's canals (74). They accommodate blood vessels and nerves as well (45, 73). The osteocytes and canaliculi are embedded between the concentric lamellae (72). Presumably, the arrangement of osteons influences the mechanical properties. In the femoral diaphysis for instance osteons run mainly parallel to the axis of the shaft (45), which might be one of the likely causes of transverse isotropy found in this region (75). This attribute represents a specific material symmetry as explained in chapter 2.2.3. The intrinsic structure of osteons also influences the capability of the specific bone segment to better resist tensile or compressive forces (69).

In contrast to the solid structure of cortical bone, cancellous bone is porous, forming an inhomogeneous and anisotropic trabecular network surrounded by bone marrow (69, 74). This type of bone is present below the endosteum in the epiphyses as well as in the transition from cortical bone of the diaphysis to the medullary cavity. Cancellous bone accommodates no osteons (45, 76). Single trabeculae consist of parallel lamellae with osteocytes and canaliculi embedded (76). Due to the missing osteons, no Haversian or Volkmann's canals exist for the accommodation of blood vessels. Instead, nutrients are transmitted from the bone marrow by canaliculi, connected to the osteocytes (77). Besides the composition on the molecular level, the mechanical characteristics of cancellous bone depend on morphological parameters such as volume fraction, the thickness or the arrangement and orientation of trabeculae (61, 78, 79). It can exhibit a high degree of anisotropy with a stiffness varying up to tenfold in different directions (69). Prevalent stresses within the bone influence bone growth (see chapter 2.1.3), provoking the trabecular fabric to vary individually and at different sites of each specifically observed bone. The magnitude of mechanical stresses affects the density of cancellous bone while the degree and direction of principal stresses have an impact on the orientation of trabeculae (80). There is evidence of a high correlation between the number of trabeculae, BV/TV and connectivity (81). In

elderly people, the number of trabeculae as well as the connectivity decreases (69). Researchers found a dramatic effect of trabecular bone resorption on modulus and strength, i.e. 10% reduction of random bony structure led to a decrease in modulus and strength of about 40% (80). A changing trabecular structure is also believed to contribute to osteoarthritis, as the dissipation of introduced loads may be altered and thus might consequently damage the articular cartilage (80). Besides the predominant mechanical functions of the trabecular architecture, some single trabecular zones may mainly fulfil metabolic tasks (69).

As shown previously, cortical and cancellous bone types differ in compositional organization. A simple derivation of bone tissue properties within the trabeculae from the mechanical properties of cortical bone on micro scale might not be valid, although this was assumed for a long time (80). Some researchers found different Young's moduli of trabecular lamellae in comparison to cortical lamellae (82-86), but general statements on this topic are difficult to make due to the fact, that many intrinsic and extrinsic factors influence the nanoindentation method, which was used to determine Young's moduli of lamellae in the listed studies (87). On the macroscale, the distinct density-elasticity relationships for cortical and trabecular bone as reported in literature (27) are evidence not to transfer material properties from one type to another. Charlebois et al. (2010) described compact bone behaving quasi-brittle in contrast to cancellous bone behaving like elastoplastic cellular material (62).

In summary, the mechanical properties of bone result from its compositional structure on nano-, micro- and macroscale. This structure varies between anatomical sites as well as for different individuals or at various stages of age.

2.1.2 GENERAL MECHANICAL ASPECTS OF THE HUMAN FEMUR

As outlined in the previous subchapter, the femur is surrounded by a rigidity providing cortical shell, which is rather thin in the epiphyses but thickens in the diaphysis. In contrast, cancellous bone with its capability of absorbing and dissipating loads is prominent in the epiphyses but only marginally present in the diaphysis. These distinct functions in combination with the distinct locations of the different bone types suggest a material distribution that compensates for

mechanical demands in an optimized way. The mechanical interaction between bone structures, the sophisticated system of muscles as well as other soft tissues is complex (88). The variety of muscle loads acting on the femur result in a hypostatic system (45). Knowledge is mainly given by telemetric *in vivo* measurements from replacements as well as by predictions from mathematical or numerical models, occasionally involving motion analyses and force measurements on test subjects (22, 88-94).

From a kinematic point of view, the femur is part of the locomotor system, enabling complex dynamic movements such as walking, running or jumping. Being part of the hip and the knee joint the femur plays an important role in human gait. The hip joint can be regarded as a ball and socket joint (95), allowing three degrees of freedom that enable adduction and abduction, flexion and extension as well as axial rotation (96). The knee joint primarily allows for flexion and extension (96). The main kinetic functions of the human femur focused on in this study are balancing and transferring loads, which arise from static and dynamic activities.

Considering the hip joint during gait, loads are assumed to mainly result from the partial body weight as well as from the abductor muscles (45). The magnitude and angle of the resulting hip force depends on the activity. Bergmann et al. (1993) measured the hip loads *in vivo* from instrumented femoral implants. They found resulting forces of approximately 5.5 times body weight during jogging, which increased up to 8.7 times body weight when the test subjects stumbled (89). Below the cortex of the femoral head, a dense trabecular network absorbs and transfers the loads to adjacent structures (see Figure 2.2). The femoral neck, whose axis runs through the centre of the femoral head, is spatially defined by the caput-collum-diaphyseal (CCD) angle in frontal (see Figure 2.2) and the antetorsion angle in the transverse plane (45). The greater trochanter on the proximolateral side of the femur is insertion point for several muscles (45), which all introduce mechanical loads. The length and orientation of the greater trochanter, as well as the length and the CCD angle of the femoral neck plays a major role in hip joint mechanics (45). Within the femur, they affect the presence of mechanical loads and moments. Providing an example for clarification, the resulting hip force commonly causes bending stresses in the femoral neck as drawn in Figure 2.2. These stresses are balanced by a prominent trabecular network.

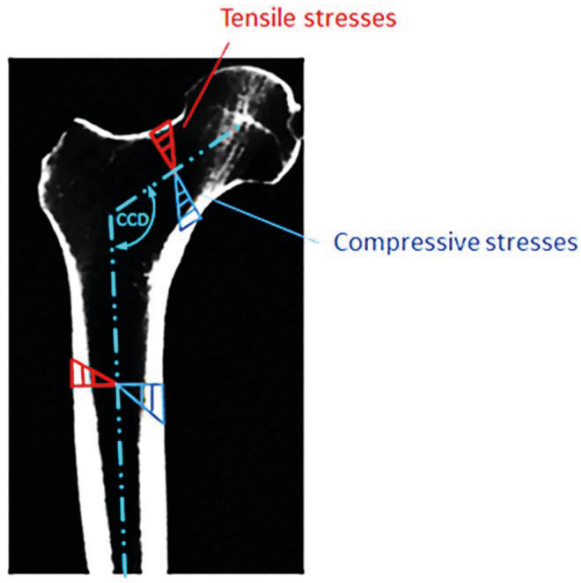

FIGURE 2.2: BENDING STRESSES IN THE FEMORAL NECK AND IN THE DIAPHYSIS.

The respective trabeculae absorb the resulting tensile forces on the proximolateral and compressive forces on the mediodistal portion of the femoral neck (45). In this context, a distorted CCD angle, as it is the case for patients with coxa vara or coxa valga, can tremendously change the stress condition within the femoral neck and consequently affects the pattern of resulting forces (45). It can likewise alter the distribution of trabecular structure. In femora without a distinctive coxa valga for instance, a Ward's triangle can be observed between compressive and tensile bundle (45), which is a less dense region where lower mechanical stresses are present. Besides the described bending moment and a certain presence of axial forces within the femoral neck introduced by the pelvitrochanteric muscles, there is evidence of a high amount of shear forces of up 3.8 times body weight during running, which might be responsible for femoral neck stress fractures in long-distance runners and military recruits (94). These shear forces are reduced in the further anatomical pathway of the proximal femur due to muscle activity (88).

In the metaphyseal transition between proximal femur and diaphysis, the thickness of the cortical shell increases while the amount of trabecular structure decreases. The femoral shaft with its thick cortical diaphysis looks straight in frontal plane while it is curved in sagittal plane (45). The ridge called *linea aspera* on the posterior side geometrically stiffens the femoral shaft as it increases its bending

resistance (45). This is essential since the femoral shaft is exposed to medialward bending stresses, resulting in compressive stresses on the medial and tensile stresses on the lateral side (45) as illustrated in Figure 2.2. In the centre of the shaft, these stresses vanish, obviating the need for supporting bone material within the medullary cavity. The bending stresses increase with the employment of adductor muscles. In contrast, the iliotibial band decreases the bending stresses within the shaft (45, 97). Attached at the fasciae latae and gluteus maximus muscle it runs parallel to the lateral femoral shaft (96, 98), acting as a tension belt by counteracting the moment, which is induced by the resulting hip force (45, 97). From isometric measurements on subjects with instrumented implants, Lu et al. (1997) confirmed the compressive forces within the femoral shaft being increased while bending stresses are decreased due to respective muscle activity (93). Compared to the proximal and distal portion of the femur, the internal axial and shear loads are reduced in the diaphysis (88). Taylor et al. (2001) investigated the compressive forces and bending moments in the femoral shaft telemetered from replacements during various activities, such as walking, jogging, stair climbing and descending, standing or jumping. They found the highest magnitude of axial forces during jogging, with a peak of 3.6 times body weight. The bending moments around mediolateral axis as well as anteroposterior axis was highest during jogging as well with a higher peak around the anteroposterior axis. The axial torque was comparably low (92). Other researchers found no considerable impact of muscle activity on the torsional moment (88).

Continuing distally, the femur features a metaphyseal region in which the thickness of cortical bone decreases while the amount of trabecular fabric increases. The distal epiphysis is characterized by its prominent medial and lateral condyles as components of the knee joint. Both condyles are of slightly different shape, according to the individual sequence of motion being likewise defined by other factors, such as the curvature of the tibial plateau or the system of cruciate ligaments (45). The knee joint follows a complicated rolling and sliding movement with the centre of rotation changing from flexion to extension. Following the different centre points in time, a curve can be drawn, which differs individually (45). The menisci of the knee joint enlarge the contact surface and thereby the range of resulting knee forces in sagittal plane (45, 95). With respect to the specific movements the muscle activity is in general very complex, leading to a multiple

hypostatic condition, which cannot be explicitly determined (45). There is evidence that the location of resulting knee forces in frontal plane is shifted medialwards. The radiodensity is higher in the medial compartment (45), indicating a higher presence of loads the bone has to resist here. Besides medial and lateral condyles forming a part of the knee joint together with the tibia, there is another knee component: the femoropatellar joint. It is located on the anterior part of the distal femur in the centre of medial and lateral condyle. The patella redirects the forces of the quadriceps femoris muscle resulting in pressure on the femoral articular surface (45, 95). Regarding the loading condition in the distal epiphysis, kinematic measurements during running yielded an elevated torsional moment resulting from external rotation (94). There is also evidence of elevated bending moments around the mediolateral axis (94) being consistent with mathematical considerations (88). In comparison with other femoral parts, elevated axial compressive forces of 11.4 times body weight and anteroposterior shear forces of up to 7.5 times body weight were measured in the distal epiphysis (94). These results emphasize the mechanical strength of this femoral region as well as of bone tissue in general.

In conclusion, the mechanical condition within each individual femur is very complex due to the respective individual muscle activity as well as the specific anatomy, influencing the stress conditions. *Vice versa* the stress conditions affect the structural anatomy in long term, being addressed in the following subchapter.

2.1.3 MORPHOLOGICAL ADAPTION AND FABRIC OF CANCELLOUS BONE

The common reputation of bone lacks its physiological vivacity although bone is highly innervated (99) and well known for its structural adaption to mechanical loading (45, 80, 100). A fast method for the adaption to higher loads is the storage of calcium salt (45), leading to a variation in BMD. Another slower and very complex process is called bone remodelling, in which old mineralized bone is resorbed by osteoclasts and new bone is formed by osteoblasts (100). The scientist Julius Wolff already claimed in 1892, that bone is capable of reconstructing its architecture according to its mechanical stress trajectories (44, 45). This allows cancellous bone to optimize its lightweight construction according to its mechanical demands. Furthermore, microdamages can be repaired (100). Wolff's theory was later on proven by Friedrich Pauwels, who investigated the adaption of bone structure as a consequence of new stress trajectory patterns in

photoelastic studies (45, 46). The mechanical stimulus, being responsible for bone remodelling, leads to one explanation for the variation of human's diverse bone morphology. Each individual has different mechanical preconditions, defined by parameters such as bone dimensions, bone shape, bone strength and muscle forces. These variables are not consistent throughout life, depending on external circumstances such as age, height, body weight, fitness or injuries. In other words, bone morphology changes continuously. In addition to mechanical stimuli other stimuli are known as well to affect bone homeostasis such as hormones and growth factors (100, 101). In this way, bone is also capable of responding to physiologically exceptional states such as pregnancy (101). There is also evidence for the central and peripheral neuronal control to play an important role in the regulation of the bone remodelling (73, 101).

The complex processes involved in bone remodelling result in variations of bone morphology of different individuals and at different anatomical sites. Beside volume fraction and intrinsic properties of the extracellular matrix, mechanical properties of cancellous bone depend on microstructural architecture (61). It is essential to consider fabric when the material behaviour of individual cancellous bone is investigated. From morphological measurements on the microstructure, a symmetric second rank tensor can be derived, which is called fabric tensor, characterizing the anisotropy of the microstructure of a solid component in a porous material (102-104). The eigensystem of this fabric tensor is closely related to the mechanical behaviour of bone as the eigenvectors define the orientation of principal axes whereas the eigenvalues describe the degree of orthotropy (61, 79, 104-106). Both parameters are essential for the description of homogenized material behaviour being the purpose of this study. The orientation of principal axes is also important information for the setup of μFEA, which is subject of chapter 2.3.4.

2.2 FUNDAMENTALS OF ELASTOMECHANICS

Although the inhomogeneity of bone was clarified in the previous chapter, each volume of interest, i.e. a small cortical or cancellous bone specimen, is regarded as a continuum with homogenous material distribution to establish density-elasticity relationships. Consequently, the laws of continuum mechanics apply. In this context, the first subchapter introduces the theory of elasticity, with the

formulation of Hooke's law, being a fundament for FEA. The second and third subchapters address anisotropic simplifications of material description applicable to bone. The mathematical elements introduced in the entire chapter are essential to fully conceive the scope of this study as well as to comprehend diverse steps in the methodology outlined in chapter 3.

2.2.1 THEORY OF ELASTICITY

Since bone features only low viscoelastic characteristics, it can be regarded as a linear elastic material (69), following Hooke's law of elasticity. Such materials feature a linear relation between the applied force and the resulting deformation as well as between the intrinsic stresses and strains within the elastic range.

Stresses are forces per unit area. They are classified according to the direction of the force vector acting on the regarded object (107). When the force is applied perpendicular to the stress plane, resulting stresses are called normal stresses, being present in compressive or tensile loading. When the applied force lies within the stress plane, resulting stresses are called shear stresses, which are present in shear or torsional loading. In three-dimensional space, stresses can be described by a tensor of second order:

$$\sigma_{ij} = \begin{bmatrix} \sigma_{11} & \sigma_{12} & \sigma_{13} \\ \sigma_{21} & \sigma_{22} & \sigma_{23} \\ \sigma_{31} & \sigma_{32} & \sigma_{33} \end{bmatrix} \quad (2.1)\ (108),$$

with the elements σ_{11}, σ_{22} and σ_{33} on the diagonal representing normal stresses and the offdiagonal entries describing shear stresses. Similar to the stress tensor, strains are also expressed by a tensor of second order in three-dimensional space:

$$\varepsilon_{kl} = \begin{bmatrix} \varepsilon_{11} & \varepsilon_{12} & \varepsilon_{13} \\ \varepsilon_{21} & \varepsilon_{22} & \varepsilon_{23} \\ \varepsilon_{31} & \varepsilon_{32} & \varepsilon_{33} \end{bmatrix} \quad (2.2)\ (108).$$

Accordingly, the elements on the diagonal are normal strains and the ones offdiagonal are shear strains. Normal strains are a dimensionless description of a changing length due to tension or compression whereas shear strains describe the half of the angle of deviation resulting from shear or torsional loading (107). Both,

the stress and the strain tensors are symmetric so that they are equal to their transpose. It follows that:

$$\sigma_{ij} = \sigma_{ji}, \quad \varepsilon_{kl} = \varepsilon_{lk} \tag{2.3}$$ (108).

This reduces the number of independent tensor components from nine to six each. In vector notation the three-dimensional stresses and strains can be expressed as:

$$\sigma_{ij} = \begin{bmatrix} \sigma_{11} \\ \sigma_{22} \\ \sigma_{33} \\ \sigma_{23} \\ \sigma_{13} \\ \sigma_{12} \end{bmatrix} = \begin{bmatrix} \sigma_{11} \\ \sigma_{22} \\ \sigma_{33} \\ \tau_{23} \\ \tau_{13} \\ \tau_{12} \end{bmatrix}, \quad \varepsilon_{kl} = \begin{bmatrix} \varepsilon_{11} \\ \varepsilon_{22} \\ \varepsilon_{33} \\ 2\varepsilon_{23} \\ 2\varepsilon_{13} \\ 2\varepsilon_{12} \end{bmatrix} = \begin{bmatrix} \varepsilon_{11} \\ \varepsilon_{22} \\ \varepsilon_{33} \\ \gamma_{23} \\ \gamma_{13} \\ \gamma_{12} \end{bmatrix} \tag{2.4}$$ (107, 108).

Hooke's law for elastic materials in three-dimensional space combines the stress vector σ_{ij} and the strain vector ε_{kl} by a Cartesian tensor of fourth order C_{ijkl} (109). This can be expressed as:

$$\begin{bmatrix} \sigma_{11} \\ \sigma_{22} \\ \sigma_{33} \\ \tau_{23} \\ \tau_{13} \\ \tau_{12} \end{bmatrix} = \begin{bmatrix} \mathrm{C}_{1111} & \mathrm{C}_{1122} & \mathrm{C}_{1133} & \mathrm{C}_{1123} & \mathrm{C}_{1113} & \mathrm{C}_{1112} \\ \mathrm{C}_{2211} & \mathrm{C}_{2222} & \mathrm{C}_{2233} & \mathrm{C}_{2223} & \mathrm{C}_{2213} & \mathrm{C}_{2212} \\ \mathrm{C}_{3311} & \mathrm{C}_{3322} & \mathrm{C}_{3333} & \mathrm{C}_{3323} & \mathrm{C}_{3313} & \mathrm{C}_{3312} \\ \mathrm{C}_{2311} & \mathrm{C}_{2322} & \mathrm{C}_{2333} & \mathrm{C}_{2323} & \mathrm{C}_{2313} & \mathrm{C}_{2312} \\ \mathrm{C}_{1311} & \mathrm{C}_{1322} & \mathrm{C}_{1333} & \mathrm{C}_{1323} & \mathrm{C}_{1313} & \mathrm{C}_{1312} \\ \mathrm{C}_{1211} & \mathrm{C}_{1222} & \mathrm{C}_{1233} & \mathrm{C}_{1223} & \mathrm{C}_{1213} & \mathrm{C}_{1212} \end{bmatrix} \cdot \begin{bmatrix} \varepsilon_{11} \\ \varepsilon_{22} \\ \varepsilon_{33} \\ \gamma_{23} \\ \gamma_{13} \\ \gamma_{12} \end{bmatrix} \tag{2.5}$$.

The establishment of this relationship is one essential step in FEA. In abbreviated form, equation 2.5 can be expressed as:

$$\sigma_{ij} = \mathrm{C}_{ijkl} \cdot \varepsilon_{kl} \tag{2.6}$$ (109, 110).

The tensor of fourth order is called stiffness tensor. It consists of 36 components representing the material-specific elastic behaviour. In other words, it determines the material specific deformation of an object on a certain stress level. The inverse of the stiffness tensor is called compliance tensor $\mathrm{K}_{ijkl} = \mathrm{C}_{ijkl}{}^{-1}$, whose 36 components consist of the material-specific elastic constants such as Young's moduli, Poisson's ratios and shear moduli. Using this description Hooke's law can be expressed as:

$$\varepsilon_{kl} = \mathrm{K}_{ijkl} \cdot \sigma_{ij} \tag{2.7}$$ (107).

2.2.2 ORTHOTROPIC SYMMETRY

Structural stiffness of bone is determined by its intrinsic material properties, its architecture as well as its boundary conditions such as muscle and gravitational forces (108). It was demonstrated in the previous chapter, that as soon as the intrinsic elastic constants of the material are known, the three-dimensional relation between stresses and strains can be computed.

Bone shows anisotropic material behaviour with its elastic constants and its strength being of higher magnitude in preferential directions. This is advantageous, since anisotropic materials accommodate high stiffness in principal stress directions at comparatively low weight, resulting in an intrinsic material optimization (108). In contrast, an isotropic material shows equal material behaviour in all directions and thereby possesses the highest possible rank in material symmetry (107). As mentioned in chapter 1, bone can fairly be assumed as orthotropic (25-29, 110).

Such material is characterized by three perpendicular planes of symmetry (107, 108), reducing the 36 independent components of the compliance tensor. The remaining elastic constants being aligned within a Cartesian coordinate system are three Young's moduli (E_1, E_2, E_3), three shear moduli (G_{23}, G_{13}, G_{12}) and six Poisson's ratios ($\nu_{23}, \nu_{32}, \nu_{13,}, \nu_{31}, \nu_{12}, \nu_{21}$) of which three are independent. Conclusively, only nine independent elastic constants were to be determined to describe the full elastic material behaviour depicted by the orthotropic compliance tensor K_{Ortho}:

$$K_{Ortho} = \begin{bmatrix} \frac{1}{E_1} & -\frac{\nu_{12}}{E_1} - & -\frac{\nu_{13}}{E_1} & 0 & 0 & 0 \\ -\frac{\nu_{21}}{E_2} & \frac{1}{E_2} & -\frac{\nu_{23}}{E_2} & 0 & 0 & 0 \\ -\frac{\nu_{31}}{E_3} & -\frac{\nu_{32}}{E_3} & \frac{1}{E_3} & 0 & 0 & 0 \\ 0 & 0 & 0 & \frac{1}{G_{23}} & 0 & 0 \\ 0 & 0 & 0 & 0 & \frac{1}{G_{31}} & 0 \\ 0 & 0 & 0 & 0 & 0 & \frac{1}{G_{12}} \end{bmatrix} \quad (2.8)\ (62).$$

Involving equation 2.7 and 2.8, Hooke's law for orthotropic materials can be expressed as:

$$\begin{bmatrix}\varepsilon_{11}\\ \varepsilon_{22}\\ \varepsilon_{33}\\ \gamma_{23}\\ \gamma_{13}\\ \gamma_{12}\end{bmatrix} = \begin{bmatrix} \frac{1}{E_1} & -\frac{\nu_{12}}{E_1} & -\frac{\nu_{13}}{E_1} & 0 & 0 & 0 \\ -\frac{\nu_{21}}{E_2} & \frac{1}{E_2} & -\frac{\nu_{23}}{E_2} & 0 & 0 & 0 \\ -\frac{\nu_{31}}{E_3} & -\frac{\nu_{32}}{E_3} & \frac{1}{E_3} & 0 & 0 & 0 \\ 0 & 0 & 0 & \frac{1}{G_{23}} & 0 & 0 \\ 0 & 0 & 0 & 0 & \frac{1}{G_{31}} & 0 \\ 0 & 0 & 0 & 0 & 0 & \frac{1}{G_{12}} \end{bmatrix} \cdot \begin{bmatrix}\sigma_{11}\\ \sigma_{22}\\ \sigma_{33}\\ \tau_{23}\\ \tau_{13}\\ \tau_{12}\end{bmatrix} \quad (2.9).$$

With respect to patient-specific FEA, the user needs to specify the elastic constants of the compliance matrix to enable the calculation of deformations and strains arising from a defined loading condition. For a density-based formulation of elastic constants, the FEA software needs to adjust the material constants for each node of the finite elements, according to the specific image intensity involved. The material laws established in this work are essential for this assignment. Subsequently, the elastic constants are regarded more specifically.

The Young's modulus of a material describes the linear relation between normal stresses and normal strains:

$$E_i = \frac{\sigma_{ii}}{\varepsilon_{ii}} \quad (2.10)\ (107)$$

The normal stress σ_{ii} is defined by the normal force F_i divided by the cross-section area A_i:

$$\sigma_{ii} = \frac{F_i}{A_i} \quad (2.11)\ (107).$$

The normal strain is defined as the change in length δ_i divided by the initial length L_i:

$$\varepsilon_{ii} = \frac{\delta_i}{L_i} \quad (2.12)\ (107)$$

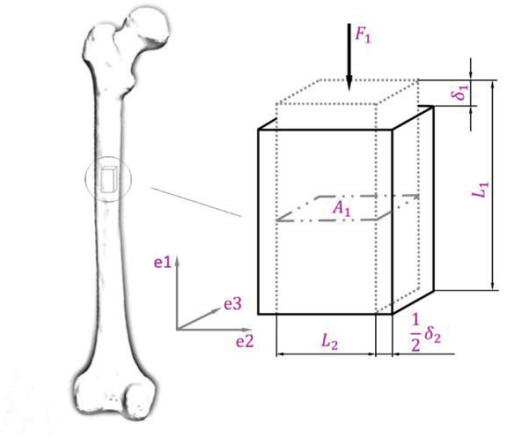

FIGURE 2.3: COMPRESSIVE LOADS APPLIED ON A FEMORAL SECTION. THE APPLIED FORCE CAUSES COMPRESSION OF THE VOLUME IN LONGITUDINAL DIRECTION AND EXTENSION IN LATERAL DIRECTION.

Conclusively, the orthotropic Young's moduli in each direction can be calculated by following equations:

$$E_1 = \frac{F_1 \cdot L_1}{A_1 \cdot \delta_1}, \quad E_2 = \frac{F_2 \cdot L_2}{A_2 \cdot \delta_2}, \quad E_3 = \frac{F_3 \cdot L_3}{A_3 \cdot \delta_3} \qquad \text{(2.13-2.15) (107).}$$

For clarification, Figure 2.3 illustrates a normal load case, in which the Force F_1 is applied on a bone sample with the cross-section area A_1. The force is applied into direction $\mathrm{e1}$, causing the compressive deformation δ_1. This scenario reflects the influence of the Young's modulus E_1. Young's Moduli E_2 and E_3 apply to the corresponding load cases in direction $\mathrm{e2}$ and $\mathrm{e3}$.

During deformation solid materials attempt to maintain their volume (107). Figure 2.3 demonstrates this phenomenon as the material attempts to maintain its volume by expanding to the sides while it is longitudinally compressed. The Poisson's ratio is a quantitative description of this behaviour. Mathematically, it expresses the negative relation between lateral and longitudinal strain as denoted in equation 2.16:

$$\nu_{ij} = -\frac{\varepsilon_{jj}}{\varepsilon_{ii}} \qquad \text{(2.16) (107).}$$

By combining equation 2.12 and 2.16, three distinct required orthotropic Poisson's ratios can be expressed as:

$$\nu_{23} = \frac{\frac{\delta_3}{L_3}}{\frac{\delta_2}{L_2}}, \qquad \nu_{13} = \frac{\frac{\delta_3}{L_3}}{\frac{\delta_1}{L_1}}, \qquad \nu_{12} = \frac{\frac{\delta_2}{L_2}}{\frac{\delta_1}{L_1}}, \qquad \text{(2.17-2.19).}$$

According to equation 2.8, the orthotropic compliance tensor contains six different Poisson's ratios of which three are dependent on other constants within the matrix, as denoted in equations 2.20 to 2.22:

$$-\frac{\nu_{23}}{E_2} = -\frac{\nu_{32}}{E_3}, \quad -\frac{\nu_{13}}{E_1} = -\frac{\nu_{31}}{E_3}, \quad -\frac{\nu_{12}}{E_1} = -\frac{\nu_{21}}{E_2} \qquad \text{(2.20-2.22)(107).}$$

The indices mark the direction of the involved strains. Figure 2.3 for instance demonstrates the influence of ν_{12} as the longitudinal strain acts in direction $\mathrm{e}1$ whereas the lateral strain describes the relative deformation in direction $\mathrm{e}2$. In the same manner ν_{23} or ν_{13} apply to the corresponding deformations in the *2-3*-plane or *1-3*-plane respectively. A general interchange of subscripts is not valid for orthotropic materials, since they are not symmetric and denote different constants (111). An incompressible material features a Poisson's ratio of 0.5 (109). For common solid materials the Poisson's ratio is lower than 0.5, meaning that the volume decreases in compression (112) and the density changes accordingly due to the applied forces.

The shear modulus of a material describes the linear relation between shear stress τ_{ij} and shear strains $2\varepsilon_{ij} = \gamma_{ij}$:

$$G_{ij} = \frac{\tau_{ij}}{2\varepsilon_{ij}} = \frac{\tau_{ij}}{\gamma_{ij}} \qquad \text{(2.23)(107).}$$

Shear stresses τ_{ij} are caused by shear forces acting on the surfaces of a parallelepiped as illustrated in Figure 2.4 (left) or by a torque acting on a cylindrical surface, as illustrated in Figure 2.4 (right), in which a femoral diaphysis is twisted.

The shear strain γ_{ij} represents the angle of distortion of a respective infinitesimal rectangular portion. With a coordinate system accordingly aligned, the shear strain of orthotropic materials is composed of two portions:

$$\gamma_{ij} = \frac{\delta u}{\delta e_i} + \frac{\delta v}{\delta e_j} \qquad \text{(2.24) (109).}$$

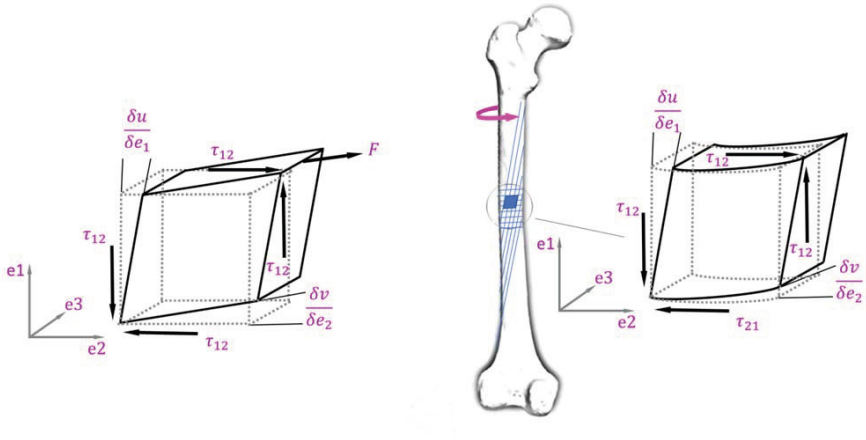

FIGURE 2.4: SHEAR LOAD CASE (LEFT) AND SHEAR LOADS APPLIED ON A FEMORAL SECTION (RIGHT).

In this context, Figure 2.4 illustrates the resulting shear strain portions in *1-2*-plane.

For torsional load cases the shear stress τ_{ij} can be expressed mathematically by the product of the torsional moment T and the lever arm r, i.e. the radius of the respective section, divided by the polar moment of inertia J_T:

$$\tau_{ij} = \frac{T \cdot r}{J_T} \qquad (2.25).$$

J_T defines the rigidity against torque caused by the geometry of the object's cross-section. From equation 2.23 and 2.25 the orthotropic shear modulus can be expressed by:

$$G_{23} = \frac{T \cdot r}{J_T \cdot \gamma_{23}}, \qquad G_{31} = \frac{T \cdot r}{J_T \cdot \gamma_{31}}, \qquad G_{12} = \frac{T \cdot r}{J_T \cdot \gamma_{12}} \qquad (2.26\text{-}2.28)\ (113)$$

The indices mark the respective shear planes. Here the interchange of subscripts is valid so that $G_{ij} = G_{ji}$. According to the orientation of the sample's principal axes, two different shear strains can in generally be evaluated in torsion at the angles $\theta = 0$ and $\theta = \frac{\pi}{2}$ with respect to a rotation around the longitudinal axis (113). For clarifying purposes, let the diaphysis of the bone in Figure 2.4 be a cylinder with circular cross-section and oriented according to the orthotropic symmetry planes. Then G_{12} can be evaluated in the illustrated *1-2*-plane ($\theta = 0$) whereas G_{13} can be evaluated in *1-3*-plane ($\theta = \frac{\pi}{2}$) according to the different shear

strains being present in the respective planes (113). Figure 2.5 illustrates the torsional shear strain results of a finite element simulation. It was conducted on a cylinder accommodating orthotropic material properties. Within the cross-section the described different shear strains are visible in the respective orthogonal planes.

The angular deformation u defines the angle of twist of a sample under torsional loads. In contrast to the shear strain, this deformation is equally distributed on the circumference of the orthotropic material as illustrated in Figure 2.6. As defined in equation 2.29, it is influenced by both shear moduli:

$$u = \frac{T \cdot r^2 \cdot l}{2 \cdot J_T} \cdot \left(\frac{1}{G_{23}} + \frac{1}{G_{12}}\right) \qquad (2.29)\ (113).$$

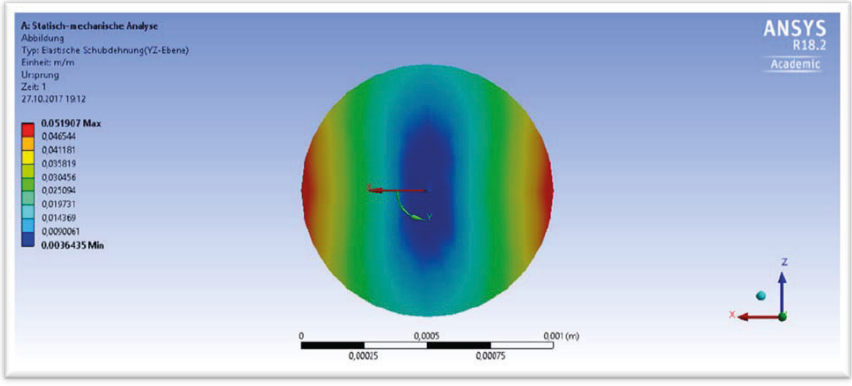

FIGURE 2.5: RESULTING SHEAR STRAINS IN AN ORTHOTROPIC CYLINDER UNDER TORSIONAL LOADS. THE SHEAR STRAINS DIFFER AT $\boldsymbol{\theta = 0}$ AND $\boldsymbol{\theta = \frac{\pi}{2}}$ WITH RESPECT TO THE ROTATION AROUND THE Y-AXIS.

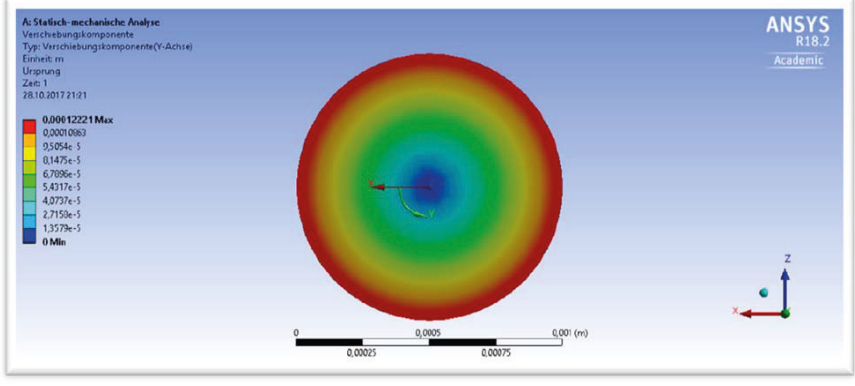

FIGURE 2.6: ANGULAR DEFORMATION OF AN ORTHOTROPIC CYLINDER UNDER TORQUE DISTRIBUTED EQUALLY ON THE CIRCUMFERENCE.

Observing the mesh deformation on the surface, the interaction of different shear moduli becomes visible as illustrated in Figure 2.7 and Figure 2.8. The drawn element in Figure 2.7 is located at $\theta = 0$. It becomes rhombical, being influenced by a low shear modulus. The element in Figure 2.8 is located at $\theta = \frac{\pi}{2}$ and contrarily influenced by a very rigid shear modulus. The perpendicularity of the element seems to be preserved while it appears to rotate on the surface, in order to ensure a unique angular deformation u of the cylinder. As a result, warping of the cylindrical cross-sections occurs.

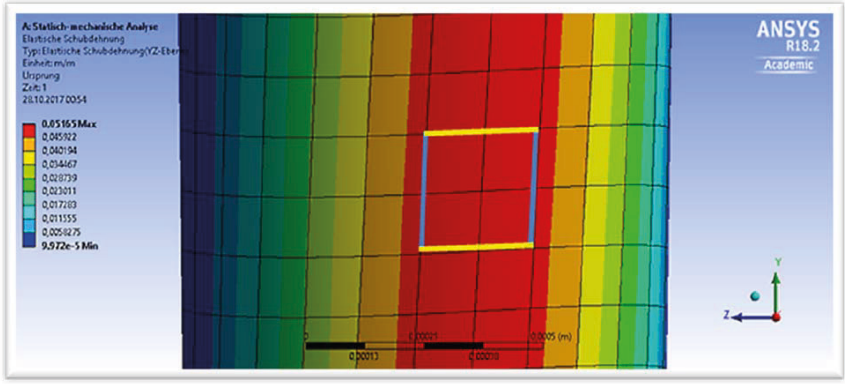

FIGURE 2.7: MESH DEFORMATION OF AN ORTHOTROPIC MATERIAL AT $\boldsymbol{\theta = 0}$, INFLUENCED BY A LOW SHEAR MODULUS. THE GEOMETRY OF THE ELEMENT DEFORMS FROM RECTANGULAR TO RHOMBICAL.

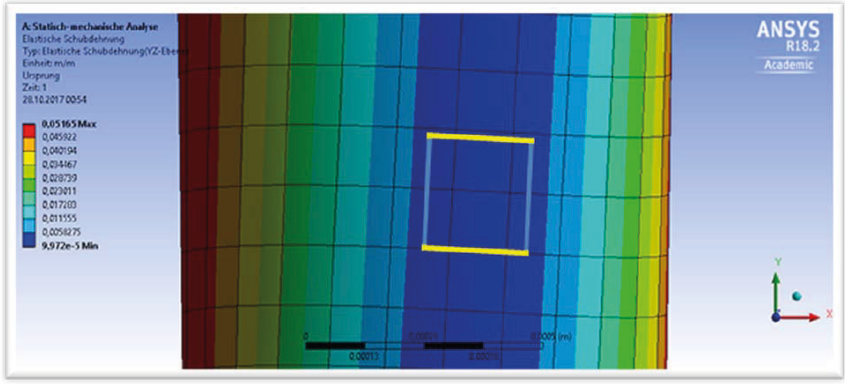

FIGURE 2.8: MESH DEFORMATION OF AN ORTHOTROPIC MATERIAL AT $\boldsymbol{\theta = \frac{\pi}{2}}$, INFLUENCED BY A HIGH SHEAR MODULUS. THE GEOMETRY OF THE ELEMENT IS COMPARABLY RIGID AND THE RECTANGULAR SHAPE SEEMS TO BE PRESERVED, WHILE THE WHOLE ELEMENT IS TILTED.

2.2.3 TRANSVERSE ISOTROPIC SYMMETRY

The material characteristics of the human femoral diaphysis can be described more simplified, since it shows transverse isotropic material behaviour (75), i.e. the longitudinal axis acts as a symmetry axis, resulting in isotropic material behaviour around the femoral shaft. Instead of nine independent material constants the transverse isotropic compliance matrix can be fully described by five distinct elastic constants: two Young's moduli (E_1, E_2), two Poisson's ratios (ν_{12}, ν_{23}) and one shear modulus (G_{12}). This reduction is derived from following dependencies, in which the subscript symbols ∥ or ⊥ indicate the considered direction either parallel or perpendicular to the orientation of the shaft.

- The Young's moduli from the isotropic *2-3*-plane are equal:

$$E_2 = E_3 = E_\perp \qquad \text{(2.30) modified from (107, 114)}$$

- The Poisson's ratios with strains in *2-3* and *3-2* direction as well as in *1-2* and *1-3* direction are identical:

$$\nu_{23} = \nu_{32} = \nu_{\perp\perp} \qquad \text{(2.31) modified from (107)}$$

$$\nu_{12} = \nu_{13} = \nu_{\parallel\perp} \qquad \text{(2.32) modified from (107)}$$

  From the relationships indicated in equations 2.21-2.22 and the equivalents expressed by equation 2.30 and 2.32 follows:

$$\nu_{21} = \nu_{31} = \nu_{\perp\parallel} \qquad \text{(2.33).}$$

- The shear moduli of the *1-2*-plane and the *1-3*-plane are equal:

$$G_{12} = G_{13} = G_{\parallel\perp} \qquad \text{(2.34) modified from (107, 114)}$$

- Due to the isotropic symmetry the third shear modulus is defined by the dependency between the respective Young's modulus E_2 and Poisson's ratio ν_{23}:

$$G_{23} = G_{\perp\perp} = \frac{E_2}{2 \cdot (1 + \nu_{23})} \qquad \text{(2.35) modified from (107, 114)}$$

Following the described relations, the transverse isotropic compliance matrix can be expressed as:

$$K_{TransIso} = \begin{bmatrix} \frac{1}{E_1} & -\frac{\nu_{12}}{E_1} - & -\frac{\nu_{12}}{E_1} & 0 & 0 & 0 \\ -\frac{\nu_{21}}{E_2} & \frac{1}{E_2} & -\frac{\nu_{23}}{E_2} & 0 & 0 & 0 \\ -\frac{\nu_{21}}{E_2} & -\frac{\nu_{23}}{E_2} & \frac{1}{E_2} & 0 & 0 & 0 \\ 0 & 0 & 0 & \frac{2 \cdot (1+\nu_{23})}{E_2} & 0 & 0 \\ 0 & 0 & 0 & 0 & \frac{1}{G_{12}} & 0 \\ 0 & 0 & 0 & 0 & 0 & \frac{1}{G_{12}} \end{bmatrix} \quad (2.36).$$

Besides the previously described relations, another exceptional attribute is noticeable, simplifying the determination of elastic constants. In isotropic materials, as well as in the isotropic cross-sections of objects accommodating transverse isotropic material behaviour, no warping occurs in torsion provided the coordinate system is accordingly aligned with the rotational axis. In consequence, the shear strains for the determination of $G_{12} = G_{13} = G_{\parallel\perp}$ are solely defined by the angle of twist, i.e. only the blue lines would tilt due to angular deformation as illustrated in Figure 2.9. With respect to equation 2.24, $\frac{\delta v}{\delta e_j}$ becomes zero. The shear strain is then mathematically defined as:

$$\gamma_{ij} = \frac{\delta u}{\delta e_i} \quad (2.37).$$

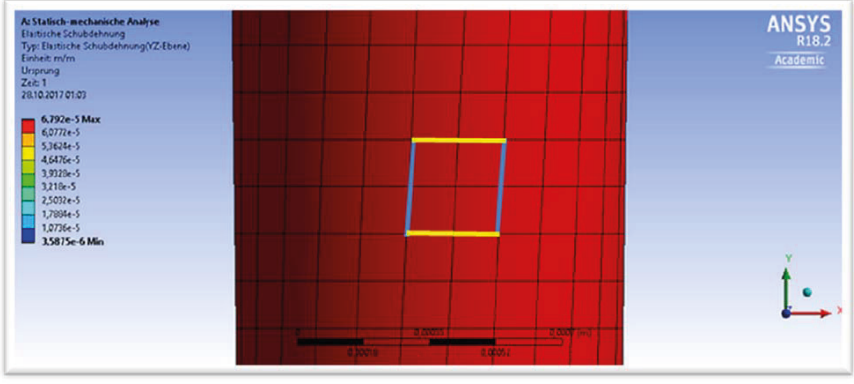

FIGURE 2.9: MESH DEFORMATION OF A TRANSVERSE ISOTROPIC MATERIAL AT $\boldsymbol{\theta = 0}$ AND $\boldsymbol{\theta = \frac{\pi}{2}}$, INFLUENCED BY AN ISOTROPIC SHEAR MODULUS. ONLY ANGULAR DEFORMATIONS OCCUR WITHOUT WARPING OF THE SAMPLE.

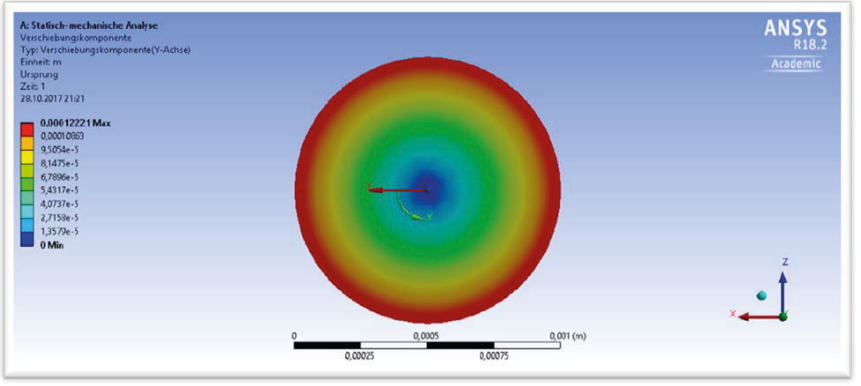

FIGURE 2.10: RESULTING SHEAR STRAINS IN THE ISOTROPIC PLANE OF A TRANSVERSELY ISOTROPIC CYLINDER UNDER TORSIONAL LOADS. THE SHEAR STRAINS ARE EQUAL AT $\boldsymbol{\theta = 0}$ AND $\boldsymbol{\theta = \frac{\pi}{2}}$ WITH RESPECT TO THE ROTATION AROUND THE Y-AXIS.

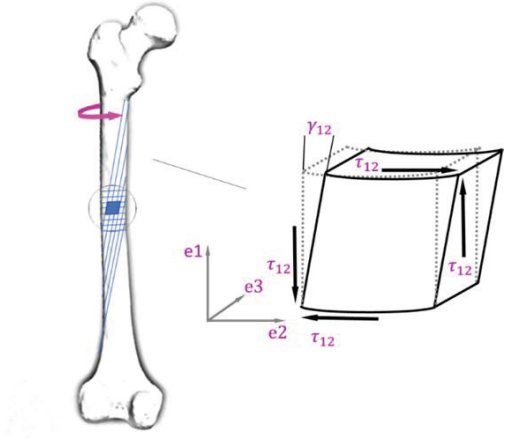

FIGURE 2.11: TORSIONAL DEFORMATION OF A FEMORAL SECTION. THE SHEAR STRAIN IS COMPLETELY DEFINED BY THE ANGULAR DEFORMATION.

Consequently, the shear strain γ_{ij} is evenly distributed on the surface of the cylinder in this case, as illustrated in the simulation results shown in Figure 2.10.

Figure 2.11 illustrates the described conditions for the previously introduced femoral diaphysis in the *1-2*-plane, in which the shear strain is completely defined by the angular deformation of the sample. This is in contrast to Figure 2.4, which illustrates the same conditions for an orthotropic material.

2.3 FUNDAMENTALS OF BONE MEASUREMENT

In this doctoral thesis, various measurements of bone properties were of importance. The first subchapter introduces common clinical methods for the determination of BMD and outlines the theory of the most suitable one for this study. The second subchapter addresses morphological investigations on cancellous bone, which are essential for the identification of the fabric eigensystem. The third subchapter introduces physical test methods for the determination of elastic properties, which is in general more complicated compared to the examination of engineering materials. Storage, the handling of the samples as well as conditions during physical testing must be well considered and are likewise topic of this subchapter. The last subchapter provides information on a numerical method to determine homogenized elastic constants of cancellous bone.

2.3.1 OSTEODENSITOMETRY

Osteodensitometry is the evaluation of BMD, usually performed to detect osteoporosis or osteopenia (115-119). In this doctoral thesis, it was used to establish density-based material laws by correlating the mineral density of a bone sample with its elastic characteristics.

There are various osteodensitometric methods available, but only some are clinically relevant nowadays. BMD can in general be evaluated by means of bone quantity from one- or two-dimensional anatomical measurements or by the assessment of bone mineral content (71), which is the matter of particular interest in this study.

It is an essential fact that different methods determine a fundamentally different formulation of BMD or BMD related specifications, being not necessarily useful for this study. This fact also complicates the comparability among one another. In order to ensure the applicability and to prevent methodological dependent systematic errors, the technique used for the establishment of elasticity-density relationships in this doctoral thesis should be identical with the method used for patients, who will be osteodensitometrically assessed with respective patient-specific FEA later on. In this context, a common clinical procedure is preferred to be chosen for the determination of BMD in this study.

Many X-ray-based methods exist for the evaluation of BMD, such as digital radiogrammetry (DXR), radiographic photodensitometry, radiographic absorptiometry (RA), single-photon absorptiometry (SPA), dual-photon absorptiometry (DPA), single energy X-ray absorptiometry (SXA), dual energy X-ray absorptiometry (DXA), peripheral dual energy X-ray absorptiometry (pDXA), quantitative computed tomography (QCT) and peripheral quantitative computed tomography (pQCT) (71). Some are even capable of morphometric evaluations such as morphometric X-ray absorptiometry (MXA) (71) or high resolution peripheral quantitative computed tomography (HR-pQCT) (64, 119-121). The underlying principles of all methods are far beyond the scope of this doctoral thesis. The interested reader is referred to Bonnick et al. (2006) (71) for detailed information on various techniques.

For clinical evaluation of BMD, DXA has become gold-standard (74, 122) measuring areal BMD on filtered two-dimensional projections of the bone (71, 74) with high precision at an extremely low radiation exposure (71). The projections however bias the extraction of geometrical features and superimpose different bone layers also including cortical and cancellous bone (74). Such assessment is incapable of determining the physical volumetric BMD, as intended in this study. Instead, it provides only surrogate information, enabling a quantitative comparison with respective specifications of a healthy population. The same is true for quantitative ultrasound (QUS) being a radiationless clinically relevant technique. Here, bone density is evaluated by the speed of sound (SOS) and broadband ultrasound attenuation (BUA) (67, 71, 122). A description of spatially defined, physical density is not feasible in this context.

In contrast, QCT concretely measures the volumetric content of bone minerals (118, 123). The densitometric properties of the spatially defined bone volume can be directly correlated to the elastic properties of the associated bone specimen, allowing for a precise formulation of density-elasticity relationships. Certainly, this also involves a differentiation between cortical and trabecular bone (118, 122, 123). The resulting volumetric radiological BMD measured from QCT is comparable to physical ash density (38). This is advantageous since results can be compared to other studies, determining bone density from physical

measurements. Further information on ash and other physical densities is given in chapter 3.6.2.

The fundamental principle of QCT is a densitometric calibration of a common CT dataset, quantifying the correlation between BMD and image intensities. For this purpose, the patient is scanned together with a calibration object, containing dipotassium phosphate (118, 124) or hydroxyapatite (123). The calibration object absorbs radiation similarly to bone (95).The Hounsfield units (HUs) being measured in the image volume of the surrogate material of the phantom provide information on the scan calibration, which allow the conclusion of BMD from HUs measured in bone representing voxels (118). Since the underlying calibration data of the surrogate materials is independent from the CT scanner, the method permits direct comparisons between different devices (95). The radiation exposure is higher in QCT compared to DXA or QUS, yet a precise extraction of the femoral anatomy is needed for the generation of a patient-specific finite element model, which requires a three-dimensionally scan of the femur anyway. Both attempts can be simply combined so that the determination of BMD by QCT does not necessarily result in additional exposure.

HR-pQCT, which is an improvement of QCT, additionally allows for morphological investigations but requires a higher image resolution compared to common clinical CT scanners (64, 119, 121). This is linked to an increased radiation dose limiting its applicability to the examination of peripheral bone, such as radius or tibia as conducted in (119) and (120) as well as to the investigation of cadaveric bone from other anatomical sites in preclinical studies (64, 125). Conclusively, it was not in conformity with the scope of this doctoral thesis, since the pre-clinical osteodensitometric method was intended to be in agreement to the later used clinical method as outlined previously.

2.3.2 MORPHOLOGICAL INVESTIGATIONS

In contrast to the limitations of high-resolution imaging for osteodensitometric measurements, morphological investigations of trabecular fabric are indispensable during the further course of this doctoral thesis. Respective image data can be acquired form high-resolution computed tomography (HRCT) scanners or from micro computed tomography (µCT) scanners, which are the gold standard.

Various morphological parameters can be derived from digital image analysis, such as trabecular thickness (Tb.Th), BV/TV, bone surface density (BS/BV), intertrabecular spacing (Tb.Sp), trabecular number (Tb.N) or connectivity (61, 126), some being particularly important for this study. Tb.Sp for instance is a measure of space between trabeculae filled by bone marrow (126). This parameter was used to assess the continuum assumption for each sample as outlined in chapter 3.7.1. The BV/TV is another essential parameter, characterizing the bone volume density of a volume of interest (VOI). It can be mathematically expressed as the bone volume (BV), defined by all bone representing voxels, over the total volume (TV), being the sum of all voxels in the VOI representing bone volume and bone marrow. Together with the degree of bone mineralization it determines the magnitude of BMD (61). It also influences the calculation time of µFEA, as it increases the number of bone elements. µFEA is further described in chapter 2.3.4.

In addition to the previously outlined parameters, the architectural anisotropy is of particular interest to this study, as it is essential to define the orientation and degree of orthotropy for each bone sample. This is necessary to assign boundary conditions prior to the microstructural examination of bone samples with µFEA as described in chapter 2.3.4. In addition, material properties of patient-specific finite element models need to be mapped according to the principal stress directions within each zone. Conclusively, the orthotropic density-elasticity relationships determined in this doctoral thesis are inevitably linked to a vectorial description of orthotropic trabecular orientation.

The fabric eigensystem, which characterizes the orthotropy of bone as described in chapter 2.1.3, can be measured by different morphological investigations. The mean intercept length (MIL) for instance was introduced by Whitehouse in 1974 (127) and is up to now the most applied method to measure fabric (105, 128). With this method the bone-marrow-interfaces are examined and the mean length between the intersections of bone and marrow is determined over different orientations (105), in order to quantify the anisotropy of trabecular surfaces (127). Initially, Whitehouse applied this method in two dimensions, resulting in an ellipse when plotted in a polar diagram (129, 130), which indicates the planar anisotropy. The method was enhanced by Harrington and Mann, who examined the VOI in three dimensions on three mutually perpendicular planes (129). This examination

resulted in a fitted ellipsoid, representing a second rank tensor M (130). Instead of an ellipsoid, the spatial tissue distribution can also be expressed by spherical Fourier series (61). Cowin specified the MIL fabric tensor as the mathematical description of the bone's anisotropy, being the inverse square root of the described tensor M (46, 80, 127). The MIL investigation is the most commonly used technique, although it disadvantageously focuses on the interfaces between bone and marrow, which can lead to undetected anisotropy for specific structures (130). Other methods focus on the volume of trabecular bone tissue only. One of these methods is called volume orientation (VO). It quantifies the bone volume around random points within the bone tissue by measuring the orientation of the longest intercept, i.e. one line from one intersection to the next intersection (127, 130). Another volume-based method is the star length distribution (SLD) (105, 127, 130). Originating from random points within the bone tissue, the orientation is measured by determining intercept lengths in various directions with more than one line (105, 127, 130), resulting in an orientation matrix. Weighting the orientation matrix with the star length leads to the fabric tensor. A small modification of SLD is the Star Volume distribution (SVD), in which the volume of the orientation is measured by considering the star lines as infinitesimal cones (105, 127, 130). In this case, the orientation matrix is weighted by the star volume to obtain the fabric tensor (127).

Different researchers tested the described fabric investigation methods (127, 128). All methods incorporate systematic divergences but no strategy is significantly better than the other ones (105, 127). Odgaard et al. (1997) emphasized, that all methods are useful for the determination of mechanical principal axes of a specimen with slightly better results for SVD and SLD. MIL was slightly worse in detecting the main principal axis (127).

2.3.3 PHYSICAL TESTING OF BONE

As outlined in chapter 2.2, the elasticity tensor accommodates normal and shear properties, which can be determined by physical measurements such as ultrasound techniques (35, 131-137) or mechanical measurements (47, 138-147).
The advantage of ultrasound techniques compared to mechanical tests is that all nine orthotropic elastic constants of one specimen can be determined but special

equipment is required and the measurement of trabecular bone is challenging (61, 63).

Mechanical tests are in general appropriate as soon as a variety of extrinsic factors or method-specific difficulties are well considered. Histological fixation methods such as the fixation in formalin are for instance known to alter mechanical properties of bone (69). Fresh bone or fresh-frozen bone is commonly used for mechanical testing (69). Mechanical experiments are likewise influenced by environmental conditions during the test. Ideal conditions are very demanding as they involve the sample being placed in Ringer's solution and maintaining body temperature during testing (69). Without placement in a bath during the experiments, it is at least essential to regulate the environmental conditions as good as possible, with an appropriate temperature between 20 and 24°C (69). Short-time dehydration during testing has no effect on material properties but long-term dehydration must be prevented by rewetting the specimen as a dried out specimen is assumed to show altered material characteristics (69).

The geometry of specimens can also affect the results of mechanical tests. Bone samples below 2 mm are not suited for mechanical testing on the macro level (69). The proportion of the sample has an effect as well, shown by investigations of the ratio between length (L) and diameter (D). For compression tests for instance, a large ratio supports unwanted bending while a small ratio increases undesirable friction effects. A ratio of L/D between one and two is recommended for such measurements. The surfaces of samples play also an important role. They should be parallel to prevent the sample from being unevenly or eccentrically loaded. Surface defects can lead to undesirable stress concentrations. Consequently, the adequate processing of bone specimens is the key to avoid systematic errors. For sample sizes of 4-5 mm lathing or milling is recommended. Dumbbell-shaped specimens are in general appropriate, enhancing the support within a machine if necessary (69).

The load application needs to be appropriately considered. Since bone is a viscoelastic material, the strain rate slightly affects the results as the specimens become stiffer at high strain rates (17, 70).

A variety of mechanical methods exist for the determination of the elastic shear modulus, but evident method-specific systematic errors decrease the number of

appropriate test methods. Standard two-plate shear tests for instance are prone to parasitic effects, as undesired tensile stresses are induced, which lead to underestimation of shear moduli (148). The determination of shear moduli from bending tests is likewise prone to be affected by local stress concentrations in the sample (148, 149). Very few researchers applied Iosipescu shear tests of bone (150-152), although a pure shear stress state can be achieved (151). This might be a consequence of the complex specimen geometry being required.

Torsion tests have likewise been used for the elastic shear measurement of bone, but it involves one difficulty, which has already been described in chapter 2.2.2.: for orthotropic materials two distinct shear moduli define the angular twist of a torsion specimen (113, 137). Appropriate measurements can in general be conducted with respective placement of single element strain gages on the sample (113), but this is difficult for bone specimens due to wet surfaces and small dimensions. Some researchers seem to disregard the distinction of different shear moduli completely as shear properties were determined solely from the angle of twist (153). Such procedure is only valid for isotropic materials or for respective symmetry planes of transverse isotropic materials as shown by finite element results in chapter 2.2.2 and 2.2.3.

Compression and tensile tests are commonly conducted to determine Young's modulus or Poisson's ratio. There is evidence of bone reacting differently to compressive or tensile loads (70, 154). In this context, compression tests are given preference in this study as respective loads are prevalent in the human femur. In comparison to tensile test specimens, the processing of samples is comparably easy and they can be kept small (69). This is of major interest since the thickness of cortical bone is limited. The method-specific systematic errors, which are known for compression tests, can be prevented or reduced by respective actions. Uneven stress distribution for instance, resulting from friction at the interface between specimen and the machine, can be reduced by lubricating the test-platens with oil (69). Underestimation of elastic constants can be caused by misalignment of the sample, which may lead to eccentric loading and the induction of undesired bending. The same is true for samples of non-perpendicular surfaces. A pivot plate can be used to reduce such errors (69). Further undesirable stress conditions can be avoided by preloading, in order to appropriately stabilize the specimen between the interfaces prior to the measurements (69).

Poisson's ratio of human cortical bone in each anatomic direction is difficult to determine with mechanical strain gauges, as the sample sizes are small and deformations of only a few microns occur when loaded mechanically. Due to the small thickness of the cortex, Reilly and Burstein (1975) excluded transverse specimens of human bone and investigated bovine bone with mechanical extensometers (138). Shahar et al. (2007) suggested the determination of anisotropic Young's modulus and Poisson's ratio with a non-contact optical method. From speckle interferometry displacements were detected from alternating laser light reflections of small mechanically loaded equine bone samples immersed in water but the resulting Poisson's ratios were much lower than reported so far (143). Another promising, optical approach is videoextensometry utilizing digital image correlation (DIC). Images of the bony object are captured during mechanical loading and the displacement is detected by comparing image data of the different images (155, 156). The approach has been known for a long time but the precision, that could be achieved with the state-of-the-art equipment at the time, was very poor (156, 157). Recently developed imaging devices enabled increased resolution of images as well as higher frame rates, paving the way for DIC in the biomechanical field. Nowadays, investigations are conducted on 2D fields or even 3D volumes (156), including the examination of extracted specimens (150) or entire bones (158). In general, it is common to use markings such as speckle patterns on the surface of the sample to optimize the results (155, 159). Such markings are particles, that are chemically or mechanically deposited on the surface of specimens (159). Since the bone surface should be kept unimpaired and the sample has to be kept moist during testing, any kind of marker setting is considered adverse or is even not feasible. Tang et al. (2015) evaluated the contrast from microstructural features of polished cortical bone specimens to be sufficient for the measurement with DIC (150).

Mechanical measurements of trabecular bone remain most challenging for several reasons. End-artefacts are for instance a common source of error in the compressive measurement of cancellous bone (49, 69, 140) and might also be relevant in the measurement of bone analogs such as polyurethane foam. On the surface of the processed specimen, the trabecular architecture is unsupported (69) due to the lack of surrounding trabeculae. As a result, end-artefacts originate from deformation and damage at the ends of the samples being in direct contact with

loading platens of the test setup (79). These artifacts can lead to an underestimation of the measured stiffness as apparently higher strains are measured beyond the ends of the sample. By embedding the ends of the sample in polymethyl methacrylate, unsupported trabeculae can be strengthened (137), but such proceeding is prone to misalignment (160) and must be well considered to prevent eccentric loading or other causes of bending stresses. Depending on the viscosity of the unset embedding material, it might also cause infiltration of the sample due to capillary effects, resulting in altered mechanical properties of the investigated sample. A better prevention of end-artefacts is the conduct of mechanical or optical extensometric measurements such as videoextensometry. Such techniques are substantially independent from compressive end-artefacts, provided that the longitudinal strain of the sample is not measured at the junction between sample and platen but closer to the center of the sample (69), where transitional stresses are balanced. Yet, there is another, more relevant difficulty for mechanical measurements of cancellous bone specimens. It is in general essential to align the specimens coincidently with the orthotropic symmetry planes of the bone in order to prevent underestimation of stiffness (69). Öhmann et al. (2006) found significantly lower Young's moduli and ultimate stresses in compressed cancellous bone specimens of up to 40 % as a result of a 20 degree off-axis alignment (161). Specimens being aligned precisely are consequently less prone to scattering (80). A precise alignment of specimens is challenging, as the material symmetries are in general not known before the examination. Morphological investigation prior to the extraction of specimens might be inevitable, which requires high resolution imaging. The unconventional orientation however would lead to a complicated extraction process, which might not even be feasible.

For cortical bone of the diaphysis the principal axis may be adequately assumed being coincident with the axis of the shaft, as it fairly represents the growth direction of osteons on the surface. Here, the osteons are longitudinally aligned, despite prevalent bending stresses, which would suggest a different growth pattern (45). The alignment of second and third principal axis may in general be of less importance in the mid-and proximal mid-diaphysis as there is evidence of this diaphyseal bone to accommodate transverse isotropic material behaviour (75). Thus, the principal axes can in general be defined in each direction of the

transverse plane. A reasonable alignment may be the choice of mediolateral and anteroposterior axes being second and third principal direction as conducted in (35, 162, 163) or axes describing the alignment of extracted specimens within the shaft, i.e. radial and circumferential orientation (35, 75, 138, 164).

2.3.4 MICROSTRUCTURAL DETERMINATION OF THE 4TH RANK ELASTICITY TENSOR

As shown in the previous chapter a proper extraction and measurement of trabecular bone is particularly demanding. This increases the desire for other than physical experiments for the investigation of elastic constants in cancellous bone. In general, the elastic constants describe the intrinsic stiffness of a material. In case of cancellous bone, homogenized constants are present on macro scale describing the extrinsic stiffness of the structure (69). There are recent approaches to determine the homogenized elastic properties from microstructural examinations. In principal, two state-of-the-art approaches are feasible.

One of them was already mentioned in chapter 1, in which the mathematical model of Zysset and Curnier (1995) (59) was used as a priori information to generate patient-specific finite element models. Such theoretic models attempt to relate the second rank fabric tensor (see chapter 2.3.2) with the fourth rank elasticity tensor (see chapter 2.2.1). Yet, the idea was not new. Related theoretical models, describing the relation between elasticity and fabric have already been introduced in the mid-eighties. Gibson et al. (1985) presented a respective model for isotropic cellular materials (61, 165). In the same year, Cowin (1985) (102) introduced general considerations, serving as groundwork for an orthotropic model of Turner and Cowin (1987) (166) as well as for the before mentioned orthotropic model of Zysset and Curnier (1995) (59), which was extended in 1998 (60, 61). Transverse isotropic models were reported likewise (63). Cowin and Yang (1997) introduced a mathematical model enabling the determination of material symmetries (61, 110, 167). The detailed explanation of mathematical relationships between elasticity and fabric tensor are beyond the scope of this doctoral thesis. The interested reader is referred to respective descriptions in the literature, such as in (61) and in (63). All mathematical models include determining variables, which need to be fitted by experiments, numerical or analytical approaches. In this context, Gross et al. (2010) calibrated some mathematical models with elastic

properties of cancellous bone derived from μFEA of a large dataset, which resulted in best predictions reported until then (63). Using such calibrated relationships between elasticity and fabric, the full homogenized elasticity tensor of cancellous bone can be approximated from simple morphological measurements on trabecular fabric, such as described in chapter 2.3.2. Considering all existing models there is evidence of the extended Zysset-Curnier model (60) being most suitable (61, 63) for this purpose.

The second approach to define homogenized elastic properties on macroscale from microstructural examinations was likewise mentioned during this work. It is the application of μFEA, which is the gold standard for the numerical analysis of bone. The method requires high-resolution image data acquired from μCT or HR-pQCT imaging (63, 121, 168, 169). By using this numerical method, the full homogenized elasticity tensor can be computed for each specimen, which is advantageous compared to mechanical test methods (63). At the same time, μFEA results of trabecular bone have been reported to be in good agreement with mechanical compression, tension and torsion tests (63, 170, 171). μFEA was even employed to enhance the prediction of fracture risk in vivo using HR-pQCT images (169).

As outlined in chapter 1, FEA is based on the discretization of an object into finite elements. The higher the number of elements the more precise is the result as it converges against an exact solution with respect to underlying mathematical formulations (18). In μFEA of cancellous bone, image voxels are commonly directly converted to cubic finite elements (63, 121, 168-171), resulting in a hexahedral volume, being called volume element (168). Conclusively, the image resolution is a limiting factor for the precision of results. This can be challenging since a certain sample size is required to ensure the continuum assumption while the number of elements is directly correlated to the computation time, which has to be kept within acceptable limits. Figure 2.12 shows a representative volume element of a cancellous bone specimen without loading (left) and under traction, resulting in respective displacements of each element (right).

Prior to the simulation, *a priori* knowledge such as tissue properties and boundary conditions need to be assigned. Commonly, tissue properties are assumed to be linearly elastic, homogeneous and isotropic for the involved trabecular elements (61, 63, 121, 168-171). Different techniques were used to define the tissue intrinsic

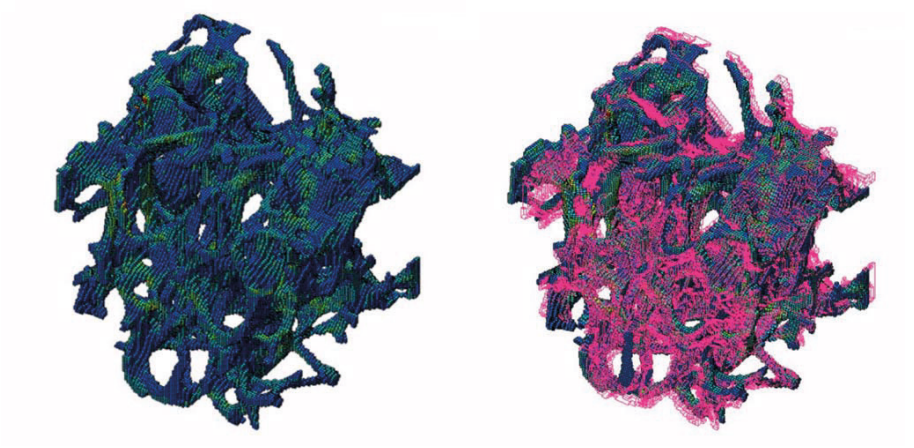

FIGURE 2.12: VOLUME ELEMENT OF BONE BEFORE (LEFT) AND AFTER LOAD APPLICATION (RIGHT). THE DEFORMATION OF ELEMENTS IS CLEARLY VISIBLE IN THE RIGHT IMAGE IN COMPARISON TO THE INITIAL POSITION OF RESPECTIVE ELEMENTS DRAWN IN PINK.

Young's modulus, such as mechanical testing, ultrasound measurements, FEA and nanoindentation (80). Mechanical testing of single trabeculae is however challenging as deformations are very small (80). Additionally, unprocessed samples do not possess a required constant cross-section and machined specimens are susceptible to surface defects, affecting the results (80). Nanoindentation is a recent method, which can achieve good results (170, 171). Yet, it is known for its sensitivity to extrinsic factors such as preparation of samples or the conduct of experiments as well as intrinsic factors like bone composition on nanoscale or the state of hydration (87, 172), which have to be well considered when data is taken from literature. Another factor to consider is the anatomical site, since Young's moduli differ between cortical and trabecular bone, between different anatomical sites as well as between different individuals. This heterogeneity is assumed to be the consequence of specific bone remodelling processes (82). The Poisson's ratio of the tissue, being likewise required for the property assignment to micro finite element models is commonly assumed (61, 63, 121, 168-170).

Boundary conditions (BC) define the mechanical loading, the degree of freedom or the displacements on the surface of the bone volume element. They have to be well considered as they influence the results (168, 173). For cancellous bone, only specific BCs are valid such as kinematic uniform BCs (KUBCs) allowing for uniform displacements only, static uniform BCs (SUBCs) allowing for uniform traction only as well as mixed uniform BCs (MUBCs) allowing for uniform

displacements and traction (168, 173). Pahr and Zysset (2008) extended these BCs by the introduction of periodicity compatible mixed uniform BCs (PMUBCs), a certain set of BCs on the surface of the volume element, allowing for specific uniform displacements and traction (168). The assignment of PMUBCs turned out to be most suitable for the simulation of cancellous bone volume elements involving orthotropic symmetry in different studies (168, 173). As expressed by equation 2.5 in chapter 2.2.1 stresses are related to strains by the 6 x 6 elasticity stiffness tensor. In consequence, the full stiffness tensor can be derived by six independent load cases (63, 173), being assigned with the respective BCs on the volume element. They involve three compressive and three shear load cases (63, 173), each load case defining one line of the stiffness tensor. The described BCs all satisfy the Hill-condition, meaning that the mechanical and energetical equivalence is fulfilled, which is necessary for the investigation of a heterogeneous material (168, 174). That involves the product of average stresses and strains on the micro-level being equivalent to those on the macro level (168, 174). Conclusively, the full stiffness tensor on macroscale can be computed from the micro finite element results by averaging the resulting stresses and strains of all involved elements as conducted in literature (63, 121, 173).

6 CONCLUSIONS AND OUTLOOK

Cortical bone samples were assessed in compression and torsion experiments using videoextensometry. Algorithms based on DIC were developed, which enabled a semi-automatic determination of all elastic constants from the images acquired during the tests. The elastic properties of cancellous samples were successfully assessed applying µFEA on µCT data. All methods were validated with polyurethane foam. The elastic material properties of cortical bone and cancellous bone as well as significant density-based material laws were in a comparable range to findings reported in literature.

The results of this thesis provide new insights about local, orthotropic mechanical properties of bone. Distinct elasticity-density laws, degrees of anisotropy, volume fraction and principal orthotropic orientations were reported for different femoral zones. The derived material laws differed across the femoral zones for both, cortical and cancellous bone, suggesting that a zone-specific formulation of elasticity-density relationships is more precise and might increase the accuracy of PSM.

The established material laws for cortical bone were of modest quality due to a limited number of samples, inaccuracies encountered in QCT as well as the imperfect extraction of specimens. Further investigations on this bone type including samples from other regions than the femoral diaphysis is recommended to gain a more comprehensive understanding of cortical material behaviour.

In contrast, the material laws of cancellous bone were in general of high statistical power. Confident correlations between elasticity and density could be confirmed for Young's moduli and shear moduli. For Poisson's ratios such relations were found occasionally, suggesting that the material behaviour is also dependent on other factors, such as the geometry of trabecular structure.

The establishment of material laws based on radiological BMD was in general susceptible to error propagation. A new determination of BMD based on BV/TV was proposed, which enhanced the quality of established material laws significantly. The procedure was only performed for cancellous bone, since no high-resolution image data was available for cortical bone but the respective approach is assumed to improve the quality of laws for cortical bone as well.

The errors in clinical osteodensitometric measurements due to surrounding tissue were quantified. It was shown that the QCT images were affected by beam hardening, leading to inconsistencies in BMD calibration. In addition, geometrical projections were distorted which may cause inaccuracies in the segmentation of bone structures in general. To eliminate such errors in clinical practice, the use of dual energy QCT is strongly recommended.

Before the empirically determined elasticity-density laws of this thesis can be employed in PSM in clinical practice, respective models need to be generated and validated. The zones defined in this thesis include artificially determined abrupt transitions, which do not mimic reality. The modelling of a smooth interpolation between zones is compulsory to reflect physiological conditions. For this purpose, it may be easier to use only one type of the established laws, linear or power laws. In case of homogenized local models, in which only one law is to be assigned, the use of the law with the most statistical power is recommended. In case of a wide range of densities, linear laws were found to be more stable.

It is assumed that imaging technologies will allow for the determination of fabric *in vivo* (61) in the future. Attempts to determine morphological parameters from radiological data were made using a flat-panel C-arm, but the accuracy of results was strongly dependent on the thickness of trabeculae (218). In MRI, high in-plane resolutions have already been obtained (16). The technical advancements of imaging modalities combined with increased computational power might therefore eliminate homogenized PSM one day.

REFERENCES

1. NEAL ML, KERCKHOFFS R: CURRENT PROGRESS IN PATIENT-SPECIFIC MODELING. BRIEFINGS IN BIOINFORMATICS 11(1): 111-126; 2009
2. TAYLOR CA, FIGUEROA C: PATIENT-SPECIFIC MODELING OF CARDIOVASCULAR MECHANICS. ANNUAL REVIEW OF BIOMEDICAL ENGINEERING 11: 109-134; 2009
3. RISSLAND P, ALEMU Y, EINAV S, RICOTTA J, BLUESTEIN D: ABDOMINAL AORTIC ANEURYSM RISK OF RUPTURE: PATIENT-SPECIFIC FSI SIMULATIONS USING ANISOTROPIC MODEL. JOURNAL OF BIOMECHANICAL ENGINEERING 131(3): 031001; 2009
4. PFEIFER B, HANSER F, SEGER M, FISCHER G, MODRE-OSPRIAN R, TILG B: PATIENT-SPECIFIC VOLUME CONDUCTOR MODELING FOR NON-INVASIVE IMAGING OF CARDIAC ELECTROPHYSIOLOGY. THE OPEN MEDICAL INFORMATICS JOURNAL 2: 32; 2008
5. SERMESANT M, CHABINIOK R, CHINCHAPATNAM P, MANSI T, BILLET F, MOIREAU P, PEYRAT J-M, WONG K, RELAN J, RHODE K: PATIENT-SPECIFIC ELECTROMECHANICAL MODELS OF THE HEART FOR THE PREDICTION OF PACING ACUTE EFFECTS IN CRT: A PRELIMINARY CLINICAL VALIDATION. MEDICAL IMAGE ANALYSIS 16(1): 201-215; 2012
6. IONASEC RI, VOIGT I, GEORGESCU B, WANG Y, HOULE H, VEGA-HIGUERA F, NAVAB N, COMANICIU D: PATIENT-SPECIFIC MODELING AND QUANTIFICATION OF THE AORTIC AND MITRAL VALVES FROM 4-D CARDIAC CT AND TEE. IEEE TRANSACTIONS ON MEDICAL IMAGING 29(9): 1636-1651; 2010
7. TANG D, YANG C, GEVA T, PEDRO J: PATIENT-SPECIFIC MRI-BASED 3D FSI RV/LV/PATCH MODELS FOR PULMONARY VALVE REPLACEMENT SURGERY AND PATCH OPTIMIZATION. JOURNAL OF BIOMECHANICAL ENGINEERING 130(4): 041010; 2008
8. MIHALEF V, IONASEC RI, SHARMA P, GEORGESCU B, VOIGT I, SUEHLING M, COMANICIU D: PATIENT-SPECIFIC MODELLING OF WHOLE HEART ANATOMY, DYNAMICS AND HAEMODYNAMICS FROM FOUR-DIMENSIONAL CARDIAC CT IMAGES. INTERFACE FOCUS 1(3): 286-296; 2011
9. CHATURVEDI A, BUTSON CR, LEMPKA SF, COOPER SE, MCINTYRE CC: PATIENT-SPECIFIC MODELS OF DEEP BRAIN STIMULATION: INFLUENCE OF FIELD MODEL COMPLEXITY ON NEURAL ACTIVATION PREDICTIONS. BRAIN STIMULATION 3(2): 65-77; 2010
10. FUENTES D, ODEN J, DILLER K, HAZLE J, ELLIOTT A, SHETTY A, STAFFORD R: COMPUTATIONAL MODELING AND REAL-TIME CONTROL OF PATIENT-SPECIFIC LASER TREATMENT OF CANCER. ANNALS OF BIOMEDICAL ENGINEERING 37(4): 763-782; 2009
11. WERNER R, EHRHARDT J, SCHMIDT R, HANDELS H: PATIENT-SPECIFIC FINITE ELEMENT MODELING OF RESPIRATORY LUNG MOTION USING 4D CT IMAGE DATA. MEDICAL PHYSICS 36(5): 1500-1511; 2009
12. DUBOWSKY SR, RASMUSSEN J, SISTO SA, LANGRANA NA: VALIDATION OF A MUSCULOSKELETAL MODEL OF WHEELCHAIR PROPULSION AND ITS APPLICATION TO MINIMIZING SHOULDER JOINT FORCES. JOURNAL OF BIOMECHANICS 41(14): 2981-2988; 2008

13. REINBOLT JA, HAFTKA RT, CHMIELEWSKI TL, FREGLY BJ: A COMPUTATIONAL FRAMEWORK TO PREDICT POST-TREATMENT OUTCOME FOR GAIT-RELATED DISORDERS. MEDICAL ENGINEERING & PHYSICS 30(4): 434-443; 2008

14. CHRISTEN P, ITO K, MÜLLER R, RUBIN MR, DEMPSTER DW, BILEZIKIAN JP, VAN RIETBERGEN B: PATIENT-SPECIFIC BONE MODELLING AND REMODELLING SIMULATION OF HYPOPARATHYROIDISM BASED ON HUMAN ILIAC CREST BIOPSIES. JOURNAL OF BIOMECHANICS 45(14): 2411-2416; 2012

15. CHRISTEN P, ITO K, DOS SANTOS AA, MÜLLER R, VAN RIETBERGEN B: VALIDATION OF A BONE LOADING ESTIMATION ALGORITHM FOR PATIENT-SPECIFIC BONE REMODELLING SIMULATIONS. JOURNAL OF BIOMECHANICS 46(5): 941-948; 2013

16. POELERT S, VALSTAR E, WEINANS H, ZADPOOR AA: PATIENT-SPECIFIC FINITE ELEMENT MODELING OF BONES. PROCEEDINGS OF THE INSTITUTION OF MECHANICAL ENGINEERS, PART H: JOURNAL OF ENGINEERING IN MEDICINE 227(4): 464-478; 2013

17. HELGASON B, TADDEI F, PÁLSSON H, SCHILEO E, CRISTOFOLINI L, VICECONTI M, BRYNJÓLFSSON S: A MODIFIED METHOD FOR ASSIGNING MATERIAL PROPERTIES TO FE MODELS OF BONES. MEDICAL ENGINEERING & PHYSICS 30(4): 444-453; 2008

18. STEINKE P: FINITE-ELEMENTE-METHODE. 1ST EDITION, 1-49, SPRINGER, BERLIN, HEIDELBERG, 2004

19. WESTERHOFF P, GRAICHEN F, BENDER A, ROHLMANN A, BERGMANN G: AN INSTRUMENTED IMPLANT FOR IN VIVO MEASUREMENT OF CONTACT FORCES AND CONTACT MOMENTS IN THE SHOULDER JOINT. MEDICAL ENGINEERING & PHYSICS 31(2): 207-213; 2009

20. NIKOOYAN A, VEEGER H, WESTERHOFF P, GRAICHEN F, BERGMANN G, VAN DER HELM F: VALIDATION OF THE DELFT SHOULDER AND ELBOW MODEL USING IN-VIVO GLENOHUMERAL JOINT CONTACT FORCES. JOURNAL OF BIOMECHANICS 43(15): 3007-3014; 2010

21. KUTZNER I, HEINLEIN B, GRAICHEN F, BENDER A, ROHLMANN A, HALDER A, BEIER A, BERGMANN G: LOADING OF THE KNEE JOINT DURING ACTIVITIES OF DAILY LIVING MEASURED IN VIVO IN FIVE SUBJECTS. JOURNAL OF BIOMECHANICS 43(11): 2164-2173; 2010

22. BERGMANN G, DEURETZBACHER G, HELLER M, GRAICHEN F, ROHLMANN A, STRAUSS J, DUDA G: HIP CONTACT FORCES AND GAIT PATTERNS FROM ROUTINE ACTIVITIES. JOURNAL OF BIOMECHANICS 34(7): 859-871; 2001

23. HELLER M, BERGMANN G, DEURETZBACHER G, DÜRSELEN L, POHL M, CLAES L, HAAS N, DUDA G: MUSCULO-SKELETAL LOADING CONDITIONS AT THE HIP DURING WALKING AND STAIR CLIMBING. JOURNAL OF BIOMECHANICS 34(7): 883-893; 2001

24. TREPCZYNSKI A, KUTZNER I, KORNAROPOULOS E, TAYLOR WR, DUDA GN, BERGMANN G, HELLER MO: PATELLOFEMORAL JOINT CONTACT FORCES DURING ACTIVITIES WITH HIGH KNEE FLEXION. JOURNAL OF ORTHOPAEDIC RESEARCH 30(3): 408-415; 2012

25. RUBIN P, RAKOTOMANANA R, LEYVRAZ P, ZYSSET P, CURNIER A, HEEGAARD J: FRICTIONAL INTERFACE MICROMOTIONS AND ANISOTROPIC STRESS DISTRIBUTION IN A FEMORAL TOTAL HIP COMPONENT. JOURNAL OF BIOMECHANICS 26(6): 725-737,735-739; 1993

26. VAN RIETBERGEN B, ODGAARD A, KABEL J, HUISKES R: DIRECT MECHANICS ASSESSMENT OF ELASTIC SYMMETRIES AND PROPERTIES OF TRABECULAR BONE ARCHITECTURE. JOURNAL OF BIOMECHANICS 29(12): 1653-1657; 1996

27. WIRTZ DC, SCHIFFERS N, PANDORF T, RADERMACHER K, WEICHERT D, FORST R: CRITICAL EVALUATION OF KNOWN BONE MATERIAL PROPERTIES TO REALIZE ANISOTROPIC FE-SIMULATION OF THE PROXIMAL FEMUR. JOURNAL OF BIOMECHANICS 33(10): 1325-1330; 2000

28. ASHMAN R, VAN BUSKIRK W: THE ELASTIC PROPERTIES OF A HUMAN MANDIBLE. ADVANCES IN DENTAL RESEARCH 1(1): 64-67; 1987

29. MARANGALOU JH, ITO K, CATALDI M, TADDEI F, VAN RIETBERGEN B: A NOVEL APPROACH TO ESTIMATE TRABECULAR BONE ANISOTROPY USING A DATABASE APPROACH. JOURNAL OF BIOMECHANICS 46(14): 2356-2362; 2013

30. FEDIDA R, YOSIBASH Z, MILGROM C, JOSCOWICZ L: FEMUR MECHANICAL SIMULATION USING HIGH-ORDER FE ANALYSIS WITH CONTINUOUS MECHANICAL PROPERTIES. PROCEEDINGS OF ICCB05-II INTERNATIONAL CONFERENCE ON COMPUTATIONAL BIOENGINEERING: 85-96; 2005

31. VICECONTI M, BELLINGERI L, CRISTOFOLINI L, TONI A: A COMPARATIVE STUDY ON DIFFERENT METHODS OF AUTOMATIC MESH GENERATION OF HUMAN FEMURS. MEDICAL ENGINEERING & PHYSICS 20(1): 1-10; 1998

32. TADDEI F, CRISTOFOLINI L, MARTELLI S, GILL H, VICECONTI M: SUBJECT-SPECIFIC FINITE ELEMENT MODELS OF LONG BONES: AN IN VITRO EVALUATION OF THE OVERALL ACCURACY. JOURNAL OF BIOMECHANICS 39(13): 2457-2467; 2006

33. PAHR DH, ZYSSET PK: FROM HIGH-RESOLUTION CT DATA TO FINITE ELEMENT MODELS: DEVELOPMENT OF AN INTEGRATED MODULAR FRAMEWORK. COMPUTER METHODS IN BIOMECHANICS AND BIOMEDICAL ENGINEERING 12(1): 45-57; 2009

34. CHEVALIER Y, PAHR D, ZYSSET PK: THE ROLE OF CORTICAL SHELL AND TRABECULAR FABRIC IN FINITE ELEMENT ANALYSIS OF THE HUMAN VERTEBRAL BODY. JOURNAL OF BIOMECHANICAL ENGINEERING 131(11): 111003; 2009

35. RHO J, HOBATHO M, ASHMAN R: RELATIONS OF MECHANICAL PROPERTIES TO DENSITY AND CT NUMBERS IN HUMAN BONE. MEDICAL ENGINEERING & PHYSICS 17(5): 347-355; 1995

36. DONG XN, GUO XE: THE DEPENDENCE OF TRANSVERSELY ISOTROPIC ELASTICITY OF HUMAN FEMORAL CORTICAL BONE ON POROSITY. JOURNAL OF BIOMECHANICS 37(8): 1281-1287; 2004

37. PENG L, BAI J, ZENG X, ZHOU Y: COMPARISON OF ISOTROPIC AND ORTHOTROPIC MATERIAL PROPERTY ASSIGNMENTS ON FEMORAL FINITE ELEMENT MODELS UNDER TWO LOADING CONDITIONS. MEDICAL ENGINEERING & PHYSICS 28(3): 227-233; 2006

38. SCHILEO E, DALL'ARA E, TADDEI F, MALANDRINO A, SCHOTKAMP T, BALEANI M, VICECONTI M: AN ACCURATE ESTIMATION OF BONE DENSITY IMPROVES THE ACCURACY OF SUBJECT-SPECIFIC FINITE ELEMENT MODELS. JOURNAL OF BIOMECHANICS 41(11): 2483-2491; 2008

39. YOSIBASH Z, PADAN R, JOSKOWICZ L, MILGROM C: A CT-BASED HIGH-ORDER FINITE ELEMENT ANALYSIS OF THE HUMAN PROXIMAL FEMUR COMPARED TO IN-VITRO EXPERIMENTS. JOURNAL OF BIOMECHANICAL ENGINEERING 129(3): 297-309; 2007

40. YOSIBASH Z, TRABELSI N, HELLMICH C: SUBJECT-SPECIFIC P-FE ANALYSIS OF THE PROXIMAL FEMUR UTILIZING MICROMECHANICS-BASED MATERIAL PROPERTIES. INTERNATIONAL JOURNAL FOR MULTISCALE COMPUTATIONAL ENGINEERING 6(5); 2008

41. TADDEI F, SCHILEO E, HELGASON B, CRISTOFOLINI L, VICECONTI M: THE MATERIAL MAPPING STRATEGY INFLUENCES THE ACCURACY OF CT-BASED FINITE ELEMENT MODELS OF BONES: AN EVALUATION AGAINST EXPERIMENTAL MEASUREMENTS. MEDICAL ENGINEERING & PHYSICS 29(9): 973-979; 2007

42. ZANNONI C, MANTOVANI R, VICECONTI M: MATERIAL PROPERTIES ASSIGNMENT TO FINITE ELEMENT MODELS OF BONE STRUCTURES: A NEW METHOD. MEDICAL ENGINEERING & PHYSICS 20(10): 735-740; 1999

43. LOTZ JC, GERHART TN, HAYES WC: MECHANICAL PROPERTIES OF TRABECULAR BONE FROM THE PROXIMAL FEMUR: A QUANTITATIVE CT STUDY. JOURNAL OF COMPUTER ASSISTED TOMOGRAPHY 14(1): 107-114; 1990

44. WOLFF J: DAS GESETZ DER TRANSFORMATION DER KNOCHEN (BERLIN A. HIRCHWILD). TRANSLATED AS: THE LAW OF BONE REMODELING. SPRINGER-VERLAG, BERLIN, 1892

45. KUMMER B: BIOMECHANIK - FORM UND FUNKTION DES BEWEGUNGSAPPARATES. 1ST EDITION, 61-334, DEUTSCHER ÄRZTEVERLAG, KÖLN, 2005

46. COWIN SC: WOLFF'S LAW OF TRABECULAR ARCHITECTURE AT REMODELING EQUILIBRIUM. JOURNAL OF BIOMECHANICAL ENGINEERING 108(1): 83-88; 1986

47. MORGAN EF, BAYRAKTAR HH, KEAVENY TM: TRABECULAR BONE MODULUS–DENSITY RELATIONSHIPS DEPEND ON ANATOMIC SITE. JOURNAL OF BIOMECHANICS 36(7): 897-904; 2003

48. CHEN G, SCHMUTZ B, EPARI D, RATHNAYAKA K, IBRAHIM S, SCHUETZ M, PEARCY M: A NEW APPROACH FOR ASSIGNING BONE MATERIAL PROPERTIES FROM CT IMAGES INTO FINITE ELEMENT MODELS. JOURNAL OF BIOMECHANICS 43(5): 1011-1015; 2010

49. HELGASON B, PERILLI E, SCHILEO E, TADDEI F, BRYNJÓLFSSON S, VICECONTI M: MATHEMATICAL RELATIONSHIPS BETWEEN BONE DENSITY AND MECHANICAL PROPERTIES: A LITERATURE REVIEW. CLINICAL BIOMECHANICS 23(2): 135-146; 2008

50. YANG H, MA X, GUO T: SOME FACTORS THAT AFFECT THE COMPARISON BETWEEN ISOTROPIC AND ORTHOTROPIC INHOMOGENEOUS FINITE ELEMENT MATERIAL MODELS OF FEMUR. MEDICAL ENGINEERING & PHYSICS 32(6): 553-560; 2010

51. BACA V, HORAK Z, MIKULENKA P, DZUPA V: COMPARISON OF AN INHOMOGENEOUS ORTHOTROPIC AND ISOTROPIC MATERIAL MODELS USED FOR FE ANALYSES. MEDICAL ENGINEERING & PHYSICS 30(7): 924-930; 2008

52. KOBER C, ERDMANN B, HELLMICH C, SADER R, ZEILHOFER H-F: CONSIDERATION OF ANISOTROPIC ELASTICITY MINIMIZES VOLUMETRIC RATHER THAN SHEAR DEFORMATION IN HUMAN MANDIBLE. COMPUTER METHODS IN BIOMECHANICS AND BIOMEDICAL ENGINEERING 9(2): 91-101; 2006

53. HELLMICH C, KOBER C, ERDMANN B: MICROMECHANICS-BASED CONVERSION OF CT DATA INTO ANISOTROPIC ELASTICITY TENSORS, APPLIED TO FE SIMULATIONS OF A MANDIBLE. ANNALS OF BIOMEDICAL ENGINEERING 36(1): 108; 2008

54. KERSH ME, ZYSSET PK, PAHR DH, WOLFRAM U, LARSSON D, PANDY MG: MEASUREMENT OF STRUCTURAL ANISOTROPY IN FEMORAL TRABECULAR BONE USING

CLINICAL-RESOLUTION CT IMAGES. JOURNAL OF BIOMECHANICS 46(15): 2659-2666; 2013

55. LARSSON D, LUISIER B, KERSH ME, DALL'ARA E, ZYSSET PK, PANDY MG, PAHR DH: ASSESSMENT OF TRANSVERSE ISOTROPY IN CLINICAL-LEVEL CT IMAGES OF TRABECULAR BONE USING THE GRADIENT STRUCTURE TENSOR. ANNALS OF BIOMEDICAL ENGINEERING 42(5): 950-959; 2014

56. MARANGALOU JH, ITO K, VAN RIETBERGEN B: A NOVEL APPROACH TO ESTIMATE TRABECULAR BONE ANISOTROPY FROM STRESS TENSORS. BIOMECHANICS AND MODELING IN MECHANOBIOLOGY 14(1): 39-48; 2015

57. SAN ANTONIO T, CIACCIA M, MÜLLER-KARGER C, CASANOVA E: ORIENTATION OF ORTHOTROPIC MATERIAL PROPERTIES IN A FEMUR FE MODEL: A METHOD BASED ON THE PRINCIPAL STRESSES DIRECTIONS. MEDICAL ENGINEERING & PHYSICS 34(7): 914-919; 2012

58. TRABELSI N, YOSIBASH Z: PATIENT-SPECIFIC FINITE-ELEMENT ANALYSES OF THE PROXIMAL FEMUR WITH ORTHOTROPIC MATERIAL PROPERTIES VALIDATED BY EXPERIMENTS. JOURNAL OF BIOMECHANICAL ENGINEERING 133(6): 061001; 2011

59. ZYSSET P, CURNIER A: AN ALTERNATIVE MODEL FOR ANISOTROPIC ELASTICITY BASED ON FABRIC TENSORS. MECHANICS OF MATERIALS 21(4): 243-250; 1995

60. ZYSSET P, GOULET R, HOLLISTER S: A GLOBAL RELATIONSHIP BETWEEN TRABECULAR BONE MORPHOLOGY AND HOMOGENIZED ELASTIC PROPERTIES. JOURNAL OF BIOMECHANICAL ENGINEERING 120(5): 640-646; 1998

61. ZYSSET PK: A REVIEW OF MORPHOLOGY–ELASTICITY RELATIONSHIPS IN HUMAN TRABECULAR BONE: THEORIES AND EXPERIMENTS. JOURNAL OF BIOMECHANICS 36(10): 1469-1485; 2003

62. CHARLEBOIS M, JIRÁSEK M, ZYSSET PK: A NONLOCAL CONSTITUTIVE MODEL FOR TRABECULAR BONE SOFTENING IN COMPRESSION. BIOMECHANICS AND MODELING IN MECHANOBIOLOGY 9(5): 597-611; 2010

63. GROSS T, PAHR DH, ZYSSET PK: MORPHOLOGY–ELASTICITY RELATIONSHIPS USING DECREASING FABRIC INFORMATION OF HUMAN TRABECULAR BONE FROM THREE MAJOR ANATOMICAL LOCATIONS. BIOMECHANICS AND MODELING IN MECHANOBIOLOGY 12(4): 793-800; 2013

64. TAGHIZADEH E, REYES M, ZYSSET P, LATYPOVA A, TERRIER A, BÜCHLER P: BIOMECHANICAL ROLE OF BONE ANISOTROPY ESTIMATED ON CLINICAL CT SCANS BY IMAGE REGISTRATION. ANNALS OF BIOMEDICAL ENGINEERING 44(8): 2505-2517; 2016

65. LEKADIR K, HAZRATI-MARANGALOU J, HOOGENDOORN C, TAYLOR Z, VAN RIETBERGEN B, FRANGI AF: STATISTICAL ESTIMATION OF FEMUR MICRO-ARCHITECTURE USING OPTIMAL SHAPE AND DENSITY PREDICTORS. JOURNAL OF BIOMECHANICS 48(4): 598-603; 2015

66. TAGHIZADEH E, CHANDRAN V, REYES M, ZYSSET P, BÜCHLER P: STATISTICAL ANALYSIS OF THE INTER-INDIVIDUAL VARIATIONS OF THE BONE SHAPE, VOLUME FRACTION AND FABRIC AND THEIR CORRELATIONS IN THE PROXIMAL FEMUR. BONE 103: 252-261; 2017

67. BARKMANN R, DENCKS S, LAUGIER P, PADILLA F, BRIXEN K, RYG J, SEEKAMP A, MAHLKE L, BREMER A, HELLER M: FEMUR ULTRASOUND (FEMUS)—FIRST CLINICAL

RESULTS ON HIP FRACTURE DISCRIMINATION AND ESTIMATION OF FEMORAL BMD. OSTEOPOROSIS INTERNATIONAL 21(6): 969-976; 2010

68. HAMEL MB, TOTH M, LEGEDZA A, ROSEN MP: JOINT REPLACEMENT SURGERY IN ELDERLY PATIENTS WITH SEVERE OSTEOARTHRITIS OF THE HIP OR KNEE: DECISION MAKING, POSTOPERATIVE RECOVERY, AND CLINICAL OUTCOMES. ARCHIVES OF INTERNAL MEDICINE 168(13): 1430-1440; 2008
69. AN YH, DRAUGHN RA: MECHANICAL TESTING OF BONE AND THE BONE-IMPLANT INTERFACE. 1ST EDITION, 3-205, CRC PRESS, BOCA RATON, 1999
70. CURREY JD: BONES: STRUCTURE AND MECHANICS. 1ST EDITION, 3-67, PRINCETON UNIVERSITY PRESS, PRINCETON, 2002
71. BONNICK SL, LEWIS LA: BONE DENSITOMETRY FOR TECHNOLOGISTS. 2ND EDITION, 1-65, SPRINGER, 2006
72. BILEZIKIAN JP, RAISZ LG, MARTIN TJ: PRINCIPLES OF BONE BIOLOGY. 2ND EDITION, 3-107, ACADEMIC PRESS, 2002
73. CHENU C: ROLE OF INNERVATION IN THE CONTROL OF BONE REMODELING. JOURNAL OF MUSCULOSKELETAL AND NEURONAL INTERACTIONS 4(2): 132; 2004
74. MITTON D, ROUX C, LAUGIER P: BONE OVERVIEW. IN: LAUGIER P, HAÏAT G: BONE QUANTITATIVE ULTRASOUND, 1-28, SPRINGER, 2011
75. ORÍAS AAE, DEUERLING JM, LANDRIGAN MD, RENAUD JE, ROEDER RK: ANATOMIC VARIATION IN THE ELASTIC ANISOTROPY OF CORTICAL BONE TISSUE IN THE HUMAN FEMUR. JOURNAL OF THE MECHANICAL BEHAVIOR OF BIOMEDICAL MATERIALS 2(3): 255-263; 2009
76. RAMACHANDRAN M: BASIC ORTHOPAEDIC SCIENCES: THE STANMORE GUIDE. 1ST EDITION, 115-122, CRC PRESS, BOCA RATON, 2006
77. RIZZO DC: FUNDAMENTALS OF ANATOMY AND PHYSIOLOGY. 4TH EDITION, 143-145, CENGAGE LEARNING, BOSTON, 2015
78. GUO X, KIM C: MECHANICAL CONSEQUENCE OF TRABECULAR BONE LOSS AND ITS TREATMENT: A THREE-DIMENSIONAL MODEL SIMULATION. BONE 30(2): 404-411; 2002
79. KEAVENY TM, MORGAN EF, NIEBUR GL, YEH OC: BIOMECHANICS OF TRABECULAR BONE. ANNUAL REVIEW OF BIOMEDICAL ENGINEERING 3(1): 307-333; 2001
80. GIBSON LJ, ASHBY MF, HARLEY BA: CELLULAR MATERIALS IN NATURE AND MEDICINE. 1ST EDITION, 126-149, CAMBRIDGE UNIVERSITY PRESS, 2010
81. GOULET RW, GOLDSTEIN SA, CIARELLI MJ, KUHN JL, BROWN M, FELDKAMP L: THE RELATIONSHIP BETWEEN THE STRUCTURAL AND ORTHOGONAL COMPRESSIVE PROPERTIES OF TRABECULAR BONE. JOURNAL OF BIOMECHANICS 27(4): 375–377, 379–389; 1994
82. ZYSSET PK, GUO XE, HOFFLER CE, MOORE KE, GOLDSTEIN SA: ELASTIC MODULUS AND HARDNESS OF CORTICAL AND TRABECULAR BONE LAMELLAE MEASURED BY NANOINDENTATION IN THE HUMAN FEMUR. JOURNAL OF BIOMECHANICS 32(10): 1005-1012; 1999
83. RHO JY, ROY ME, TSUI TY, PHARR GM: ELASTIC PROPERTIES OF MICROSTRUCTURAL COMPONENTS OF HUMAN BONE TISSUE AS MEASURED BY NANOINDENTATION. JOURNAL OF BIOMEDICAL MATERIALS RESEARCH PART A 45(1): 48-54; 1999

84. HENGSBERGER S, KULIK A, ZYSSET P: A COMBINED ATOMIC FORCE MICROSCOPY AND NANOINDENTATION TECHNIQUE TO INVESTIGATE THE ELASTIC PROPERTIES OF BONE STRUCTURAL UNITS. EUROPEAN CELLS & MATERIALS 1: 12-17; 2001

85. HENGSBERGER S, KULIK A, ZYSSET P: NANOINDENTATION DISCRIMINATES THE ELASTIC PROPERTIES OF INDIVIDUAL HUMAN BONE LAMELLAE UNDER DRY AND PHYSIOLOGICAL CONDITIONS. BONE 30(1): 178-184; 2002

86. BAYRAKTAR HH, MORGAN EF, NIEBUR GL, MORRIS GE, WONG EK, KEAVENY TM: COMPARISON OF THE ELASTIC AND YIELD PROPERTIES OF HUMAN FEMORAL TRABECULAR AND CORTICAL BONE TISSUE. JOURNAL OF BIOMECHANICS 37(1): 27-35; 2004

87. LEWIS G, NYMAN JS: THE USE OF NANOINDENTATION FOR CHARACTERIZING THE PROPERTIES OF MINERALIZED HARD TISSUES: STATE-OF-THE ART REVIEW. JOURNAL OF BIOMEDICAL MATERIALS RESEARCH PART B: APPLIED BIOMATERIALS 87(1): 286-301; 2008

88. DUDA GN, SCHNEIDER E, CHAO EY: INTERNAL FORCES AND MOMENTS IN THE FEMUR DURING WALKING. JOURNAL OF BIOMECHANICS 30(9): 933-941; 1997

89. BERGMANN G, GRAICHEN F, ROHLMANN A: HIP JOINT LOADING DURING WALKING AND RUNNING, MEASURED IN TWO PATIENTS. JOURNAL OF BIOMECHANICS 26(8): 969-990; 1993

90. TAYLOR S, PERRY J, MESWANIA J, DONALDSON N, WALKER P, CANNON S: TELEMETRY OF FORCES FROM PROXIMAL FEMORAL REPLACEMENTS AND RELEVANCE TO FIXATION. JOURNAL OF BIOMECHANICS 30(3): 225-234; 1997

91. TAYLOR M, TANNER K, FREEMAN M, YETTRAM A: STRESS AND STRAIN DISTRIBUTION WITHIN THE INTACT FEMUR: COMPRESSION OR BENDING? MEDICAL ENGINEERING & PHYSICS 18(2): 122-131; 1996

92. TAYLOR S, WALKER P: FORCES AND MOMENTS TELEMETERED FROM TWO DISTAL FEMORAL REPLACEMENTS DURING VARIOUS ACTIVITIES. JOURNAL OF BIOMECHANICS 34(7): 839-848; 2001

93. LU T-W, TAYLOR SJ, O'CONNOR JJ, WALKER PS: INFLUENCE OF MUSCLE ACTIVITY ON THE FORCES IN THE FEMUR: AN IN VIVO STUDY. JOURNAL OF BIOMECHANICS 30(11-12): 1101-1106; 1997

94. EDWARDS WB, GILLETTE JC, THOMAS JM, DERRICK TR: INTERNAL FEMORAL FORCES AND MOMENTS DURING RUNNING: IMPLICATIONS FOR STRESS FRACTURE DEVELOPMENT. CLINICAL BIOMECHANICS 23(10): 1269-1278; 2008

95. BRINCKMANN P, FROBIN W, LEIVSETH G: MUSCULOSKELETAL BIOMECHANICS. 1ST EDITION, 69-168, THIEME, 2002

96. KAPANDJI IA: FUNKTIONELLE ANATOMIE DER GELENKE - BAND 2: UNTERE EXTREMITÄT. 2ND EDITION, 2-64, FERDINAND ENKE VERLAG, STUTTGART, 1992

97. BENNINGHOFF A, GOERTTLER K: LEHRBUCH DER ANATOMIE DES MENSCHEN - MAKROSKOPISCHE UND MIKROSKOPISCHE ANATOMIE UNTER FUNKTIONELLEN GESICHTSPUNKTEN - ERSTER BAND: ALLGEMEINE ANATOMIE, CYTOLOGIE UND BEWEGUNGSAPPARAT. 11TH EDITION, 309-314, URBAN UND SCHWARZENBERG, MÜNCHEN, BERLIIN, WIEN, 1975

98. LEUTERT G, SCHMIDT W: SYSTEMATISCHE UND FUNKTIONELLE ANATOMIE FÜR MEDIZINISCHE ASSISTENZBERUFE. 10TH EDITION, 137-139, ELSEVIER, URBAN & FISCHER VERLAG, MÜNCHEN, JENA, 2004

99. SERRE C, FARLAY D, DELMAS P, CHENU C: EVIDENCE FOR A DENSE AND INTIMATE INNERVATION OF THE BONE TISSUE, INCLUDING GLUTAMATE-CONTAINING FIBERS. BONE 25(6): 623-629; 1999

100. HADJIDAKIS DJ, ANDROULAKIS II: BONE REMODELING. ANNALS OF THE NEW YORK ACADEMY OF SCIENCES 1092(1): 385-396; 2006

101. ELEFTERIOU F: NEURONAL SIGNALING AND THE REGULATION OF BONE REMODELING. CELLULAR AND MOLECULAR LIFE SCIENCES CMLS 62(19-20): 2339-2349; 2005

102. COWIN SC: THE RELATIONSHIP BETWEEN THE ELASTICITY TENSOR AND THE FABRIC TENSOR. MECHANICS OF MATERIALS 4(2): 137-147; 1985

103. COWIN SC: ANISOTROPIC POROELASTICITY: FABRIC TENSOR FORMULATION. MECHANICS OF MATERIALS 36(8): 665-677; 2004

104. RYAN TM, KETCHAM RA: ANGULAR ORIENTATION OF TRABECULAR BONE IN THE FEMORAL HEAD AND ITS RELATIONSHIP TO HIP JOINT LOADS IN LEAPING PRIMATES. JOURNAL OF MORPHOLOGY 265(3): 249-263; 2005

105. KETCHAM R, RYAN T: QUANTIFICATION AND VISUALIZATION OF ANISOTROPY IN TRABECULAR BONE. JOURNAL OF MICROSCOPY 213(2): 158-171; 2004

106. GOMBERG BR, SAHA PK, WEHRLI FW: TOPOLOGY-BASED ORIENTATION ANALYSIS OF TRABECULAR BONE NETWORKS. MEDICAL PHYSICS 30(2): 158-168; 2003

107. COWIN SC: MECHANICS OF MATERIALS. IN: COWIN SC: BONE MECHANICS HANDBOOK. 2ND EDITION, 6-1-24, CRC PRESS, BOCA RATON, 2001

108. ETH ZÜRICH: ANISOTROPIE. HTTPS://WWW1.ETHZ.CH/STRUCTURES/EDUCATION/BACHELOR/FASERVERSTAERKTE_KUNSTSTOFFE/SKRIPT/151-0363-03_ANISOTROPIE.PDF (DATE OF ACCESS: MARCH 20TH, 2013)

109. RÖSLER J, HARDERS H, BÄKER M: MECHANISCHES VERHALTEN DER WERKSTOFFE. 4TH EDITION, 34-46, SPRINGER-VERLAG, WIESBADEN, 2012

110. YANG G, KABEL J, VAN RIETBERGEN B, ODGAARD A, HUISKES R, COWN SC: THE ANISOTROPIC HOOKE'S LAW FOR CANCELLOUS BONE AND WOOD. JOURNAL OF ELASTICITY 53(2): 125-146; 1998

111. CHENG A-D: MATERIAL COEFFICIENTS OF ANISOTROPIC POROELASTICITY. INTERNATIONAL JOURNAL OF ROCK MECHANICS AND MINING SCIENCES 34(2): 199-205; 1997

112. DEMTRÖDER W: EXPERIMENTALPHYSIK 1 - MECHANIK UND WÄRME. 8TH EDITION, 157-164, SPRINGER, BERLIN, 2018

113. PAGANO N: SHEAR MODULI OF ORTHOTROPIC COMPOSITES. HTTP://WWW.DTIC.MIL/DTIC/TR/FULLTEXT/U2/A084975.PDF (DATE OF ACCESS: AUGUST, 17TH, 2017)

114. ALTENBACH H: KONTINUUMSMECHANIK: EINFÜHRUNG IN DIE MATERIALUNABHÄNGIGEN UND MATERIALABHÄNGIGEN GLEICHUNGEN. 3RD EDITION, 325-332, SPRINGER-VERLAG, BERLIN, HEIDELBERG, 2015

115. TENENHOUSE A, JOSEPH L, KREIGER N, POLIQUIN S, MURRAY T, BLONDEAU L, BERGER C, HANLEY D, PRIOR J, GROUP CR: ESTIMATION OF THE PREVALENCE OF LOW BONE DENSITY IN CANADIAN WOMEN AND MEN USING A POPULATION-SPECIFIC DXA REFERENCE STANDARD: THE CANADIAN MULTICENTRE OSTEOPOROSIS STUDY (CAMOS). OSTEOPOROSIS INTERNATIONAL 11(10): 897-904; 2000

116. LIMPAPHAYOM KK, TAECHAKRAICHANA N, JAISAMRARN U, BUNYAVEJCHEVIN S, CHAIKITTISILPA S, POSHYACHINDA M, TAECHAMAHACHAI C, HAVANOND P, ONTHUAM Y, LUMBIGANON P: PREVALENCE OF OSTEOPENIA AND OSTEOPOROSIS IN THAI WOMEN. MENOPAUSE 8(1): 65-69; 2001

117. LOOKER AC, ORWOLL ES, JOHNSTON CC, LINDSAY RL, WAHNER HW, DUNN WL, CALVO MS, HARRIS TB, HEYSE SP: PREVALENCE OF LOW FEMORAL BONE DENSITY IN OLDER US ADULTS FROM NHANES III. JOURNAL OF BONE AND MINERAL RESEARCH 12(11): 1761-1768; 1997

118. GENANT HK, BLOCK JE, STEIGER P, GLUEER C-C, SMITH R: QUANTITATIVE COMPUTED TOMOGRAPHY IN ASSESSMENT OF OSTEOPOROSIS. SEMINARS IN NUCLEAR MEDICINE 17(4): 316-333; 1987

119. HANSEN S, BECK JENSEN JE, RASMUSSEN L, HAUGE EM, BRIXEN K: EFFECTS ON BONE GEOMETRY, DENSITY, AND MICROARCHITECTURE IN THE DISTAL RADIUS BUT NOT THE TIBIA IN WOMEN WITH PRIMARY HYPERPARATHYROIDISM: A CASE-CONTROL STUDY USING HR-PQCT. JOURNAL OF BONE AND MINERAL RESEARCH 25(9): 1941-1947; 2010

120. BURGHARDT AJ, BUIE HR, LAIB A, MAJUMDAR S, BOYD SK: REPRODUCIBILITY OF DIRECT QUANTITATIVE MEASURES OF CORTICAL BONE MICROARCHITECTURE OF THE DISTAL RADIUS AND TIBIA BY HR-PQCT. BONE 47(3): 519-528; 2010

121. PISTOIA W, VAN RIETBERGEN B, LOCHMÜLLER E-M, LILL C, ECKSTEIN F, RÜEGSEGGER P: ESTIMATION OF DISTAL RADIUS FAILURE LOAD WITH MICRO-FINITE ELEMENT ANALYSIS MODELS BASED ON THREE-DIMENSIONAL PERIPHERAL QUANTITATIVE COMPUTED TOMOGRAPHY IMAGES. BONE 30(6): 842-848; 2002

122. BARONCELLI GI: QUANTITATIVE ULTRASOUND METHODS TO ASSESS BONE MINERAL STATUS IN CHILDREN: TECHNICAL CHARACTERISTICS, PERFORMANCE, AND CLINICAL APPLICATION. PEDIATRIC RESEARCH 63(3): 220-228; 2008

123. REINBOLD W-D, ADLER C, KALENDER W, LENTE R: ACCURACY OF VERTEBRAL MINERAL DETERMINATION BY DUAL-ENERGY QUANTITATIVE COMPUTED TOMOGRAPHY. SKELETAL RADIOLOGY 20(1): 25-29; 1991

124. LAVAL-JEANTET AM, ROGER B, BOUYSEE S, BERGOT C, MAZESS R: INFLUENCE OF VERTEBRAL FAT CONTENT ON QUANTITATIVE CT DENSITY. RADIOLOGY 159(2): 463-466; 1986

125. LUISIER B, DALL E, PAHR D: ORTHOTROPIC HR-PQCT-BASED FE MODELS IMPROVE STRENGTH PREDICTIONS FOR STANCE BUT NOT FOR SIDE-WAY FALL LOADING COMPARED TO ISOTROPIC QCT-BASED FE MODELS OF HUMAN FEMURS. JOURNAL OF THE MECHANICAL BEHAVIOR OF BIOMEDICAL MATERIALS 32: 287-299; 2014

126. HILDEBRAND T, LAIB A, MÜLLER R, DEQUEKER J, RÜEGSEGGER P: DIRECT THREE-DIMENSIONAL MORPHOMETRIC ANALYSIS OF HUMAN CANCELLOUS BONE: MICROSTRUCTURAL DATA FROM SPINE, FEMUR, ILIAC CREST, AND CALCANEUS. JOURNAL OF BONE AND MINERAL RESEARCH 14(7): 1167-1174; 1999

127. ODGAARD A, KABEL J, VAN RIETBERGEN B, DALSTRA M, HUISKES R: FABRIC AND ELASTIC PRINCIPAL DIRECTIONS OF CANCELLOUS BONE ARE CLOSELY RELATED. JOURNAL OF BIOMECHANICS 30(5): 487-495; 1997

128. VAN RIETBERGEN B, ODGAARD A, KABEL J, HUISKES R: RELATIONSHIPS BETWEEN BONE MORPHOLOGY AND BONE ELASTIC PROPERTIES CAN BE ACCURATELY QUANTIFIED USING HIGH-RESOLUTION COMPUTER RECONSTRUCTIONS. JOURNAL OF ORTHOPAEDIC RESEARCH 16(1): 23-28; 1998

129. INGLIS D, PIETRUSZCZAK S: CHARACTERIZATION OF ANISOTROPY IN POROUS MEDIA BY MEANS OF LINEAR INTERCEPT MEASUREMENTS. INTERNATIONAL JOURNAL OF SOLIDS AND STRUCTURES 40(5): 1243-1264; 2003

130. ODGAARD A: THREE-DIMENSIONAL METHODS FOR QUANTIFICATION OF CANCELLOUS BONE ARCHITECTURE. BONE 20(4): 315-328; 1997

131. VAN BUSKIRK W, COWIN S, WARD RN: ULTRASONIC MEASUREMENT OF ORTHOTROPIC ELASTIC CONSTANTS OF BOVINE FEMORAL BONE. JOURNAL OF BIOMECHANICAL ENGINEERING 103(2): 67-72; 1981

132. ASHMAN R, COWIN S, VAN BUSKIRK W, RICE J: A CONTINUOUS WAVE TECHNIQUE FOR THE MEASUREMENT OF THE ELASTIC PROPERTIES OF CORTICAL BONE. JOURNAL OF BIOMECHANICS 17(5): 349-361; 1984

133. YOON HS, KATZ JL: ULTRASONIC WAVE PROPAGATION IN HUMAN CORTICAL BONE—II. MEASUREMENTS OF ELASTIC PROPERTIES AND MICROHARDNESS. JOURNAL OF BIOMECHANICS 9(7): 459-462, IN459, 463-464; 1976

134. PITHIOUX M, LASAYGUES P, CHABRAND P: AN ALTERNATIVE ULTRASONIC METHOD FOR MEASURING THE ELASTIC PROPERTIES OF CORTICAL BONE. JOURNAL OF BIOMECHANICS 35(7): 961-968; 2002

135. LEE T, LAKES R, LAL A: INVESTIGATION OF BOVINE BONE BY RESONANT ULTRASOUND SPECTROSCOPY AND TRANSMISSION ULTRASOUND. BIOMECHANICS AND MODELING IN MECHANOBIOLOGY 1(2): 165-175; 2002

136. BERNARD S, GRIMAL Q, LAUGIER P: ACCURATE MEASUREMENT OF CORTICAL BONE ELASTICITY TENSOR WITH RESONANT ULTRASOUND SPECTROSCOPY. JOURNAL OF THE MECHANICAL BEHAVIOR OF BIOMEDICAL MATERIALS 18: 12-19; 2013

137. ASHMAN RB, CORIN JD, TURNER CH: ELASTIC PROPERTIES OF CANCELLOUS BONE: MEASUREMENT BY AN ULTRASONIC TECHNIQUE. JOURNAL OF BIOMECHANICS 20(10): 979–983, 985–986; 1987

138. REILLY DT, BURSTEIN AH: THE ELASTIC AND ULTIMATE PROPERTIES OF COMPACT BONE TISSUE. JOURNAL OF BIOMECHANICS 8(6): 393-396, IN399-IN311, 397-405; 1975

139. LOTZ JC, GERHART TN, HAYES WC: MECHANICAL PROPERTIES OF METAPHYSEAL BONE IN THE PROXIMAL FEMUR. JOURNAL OF BIOMECHANICS 24(5): 317-325, 327-329; 1991

140. KEAVENY TM, PINILLA TP, CRAWFORD RP, KOPPERDAHL DL, LOU A: SYSTEMATIC AND RANDOM ERRORS IN COMPRESSION TESTING OF TRABECULAR BONE. JOURNAL OF ORTHOPAEDIC RESEARCH 15(1): 101-110; 1997

141. CARTER DR, HAYES WC: THE COMPRESSIVE BEHAVIOR OF BONE AS A TWO-PHASE POROUS STRUCTURE. THE JOURNAL OF BONE AND JOINT SURGERY 59(7): 954-962; 1977

142. KELLER TS: PREDICTING THE COMPRESSIVE MECHANICAL BEHAVIOR OF BONE. JOURNAL OF BIOMECHANICS 27(9): 1159-1168; 1994

143. SHAHAR R, ZASLANSKY P, BARAK M, FRIESEM A, CURREY J, WEINER S: ANISOTROPIC POISSON'S RATIO AND COMPRESSION MODULUS OF CORTICAL BONE DETERMINED BY SPECKLE INTERFEROMETRY. JOURNAL OF BIOMECHANICS 40(2): 252-264; 2007

144. MATSUURA M, ECKSTEIN F, LOCHMÜLLER E-M, ZYSSET PK: THE ROLE OF FABRIC IN THE QUASI-STATIC COMPRESSIVE MECHANICAL PROPERTIES OF HUMAN TRABECULAR BONE FROM VARIOUS ANATOMICAL LOCATIONS. BIOMECHANICS AND MODELING IN MECHANOBIOLOGY 7(1): 27-42; 2008

145. LI S, DEMIRCI E, SILBERSCHMIDT VV: VARIABILITY AND ANISOTROPY OF MECHANICAL BEHAVIOR OF CORTICAL BONE IN TENSION AND COMPRESSION. JOURNAL OF THE MECHANICAL BEHAVIOR OF BIOMEDICAL MATERIALS 21: 109-120; 2013

146. REILLY DT, BURSTEIN AH, FRANKEL VH: THE ELASTIC MODULUS FOR BONE. JOURNAL OF BIOMECHANICS 7(3): 271-272, IN279-IN212, 273-275; 1974

147. BROWN TD, FERGUSON AB: MECHANICAL PROPERTY DISTRIBUTIONS IN THE CANCELLOUS BONE OF THE HUMAN PROXIMAL FEMUR. ACTA ORTHOPAEDICA SCANDINAVICA 51(1-6): 429-437; 1980

148. GRÉDIAC M, DUFORT L: EXPERIMENTAL EVIDENCE OF PARASITIC EFFECTS IN THE SHEAR TEST ON SANDWICH BEAMS. EXPERIMENTAL MECHANICS 42(2): 186-193; 2002

149. CHOI K, KUHN JL, CIARELLI MJ, GOLDSTEIN SA: THE ELASTIC MODULI OF HUMAN SUBCHONDRAL, TRABECULAR, AND CORTICAL BONE TISSUE AND THE SIZE-DEPENDENCY OF CORTICAL BONE MODULUS. JOURNAL OF BIOMECHANICS 23(11): 1103-1113; 1990

150. TANG T, EBACHER V, CRIPTON P, GUY P, MCKAY H, WANG R: SHEAR DEFORMATION AND FRACTURE OF HUMAN CORTICAL BONE. BONE 71: 25-35; 2015

151. TURNER C, WANG T, BURR D: SHEAR STRENGTH AND FATIGUE PROPERTIES OF HUMAN CORTICAL BONE DETERMINED FROM PURE SHEAR TESTS. CALCIFIED TISSUE INTERNATIONAL 69(6): 373-378; 2001

152. WINWOOD K, ZIOUPOS P, CURREY J, COTTON JR, TAYLOR M: STRAIN PATTERNS DURING TENSILE, COMPRESSIVE, AND SHEAR FATIGUE OF HUMAN CORTICAL BONE AND IMPLICATIONS FOR BONE BIOMECHANICS. JOURNAL OF BIOMEDICAL MATERIALS RESEARCH PART A 79(2): 289-297; 2006

153. FORD CM, KEAVENY TM: THE DEPENDENCE OF SHEAR FAILURE PROPERTIES OF TRABECULAR BONE ON APPARENT DENSITY AND TRABECULAR ORIENTATION. JOURNAL OF BIOMECHANICS 29(10): 1309-1317; 1996

154. GOLDSTEIN SA: THE MECHANICAL PROPERTIES OF TRABECULAR BONE: DEPENDENCE ON ANATOMIC LOCATION AND FUNCTION. JOURNAL OF BIOMECHANICS 20(11-12): 1055-1061; 1987

155. LECOMPTE D, SMITS A, BOSSUYT S, SOL H, VANTOMME J, VAN HEMELRIJCK D, HABRAKEN A: QUALITY ASSESSMENT OF SPECKLE PATTERNS FOR DIGITAL IMAGE CORRELATION. OPTICS AND LASERS IN ENGINEERING 44(11): 1132-1145; 2006

156. GRASSI L, ISAKSSON H: EXTRACTING ACCURATE STRAIN MEASUREMENTS IN BONE MECHANICS: A CRITICAL REVIEW OF CURRENT METHODS. JOURNAL OF THE MECHANICAL BEHAVIOR OF BIOMEDICAL MATERIALS 50: 43-54; 2015

157. ODGAARD A, LINDE F: THE UNDERESTIMATION OF YOUNG'S MODULUS IN COMPRESSIVE TESTING OF CANCELLOUS BONE SPECIMENS. JOURNAL OF BIOMECHANICS 24(8): 691-698; 1991

158. HUSSEIN AI, BARBONE PE, MORGAN EF: DIGITAL VOLUME CORRELATION FOR STUDY OF THE MECHANICS OF WHOLE BONES. PROCEDIA IUTAM 4: 116-125; 2012

159. LIONELLO G, CRISTOFOLINI L: A PRACTICAL APPROACH TO OPTIMIZING THE PREPARATION OF SPECKLE PATTERNS FOR DIGITAL-IMAGE CORRELATION. MEASUREMENT SCIENCE AND TECHNOLOGY 25(10): 107001; 2014

160. LIEVERS W, WALDMAN S, PILKEY A: MINIMIZING SPECIMEN LENGTH IN ELASTIC TESTING OF END-CONSTRAINED CANCELLOUS BONE. JOURNAL OF THE MECHANICAL BEHAVIOR OF BIOMEDICAL MATERIALS 3(1): 22-30; 2010

161. ÖHMAN C, BALEANI M, PERILLI E, DALL'ARA E, TASSANI S, BARUFFALDI F, VICECONTI M: MECHANICAL TESTING OF CANCELLOUS BONE FROM THE FEMORAL HEAD: EXPERIMENTAL ERRORS DUE TO OFF-AXIS MEASUREMENTS. JOURNAL OF BIOMECHANICS 40(11): 2426-2433; 2007

162. AUGAT P, LINK T, LANG TF, LIN JC, MAJUMDAR S, GENANT HK: ANISOTROPY OF THE ELASTIC MODULUS OF TRABECULAR BONE SPECIMENS FROM DIFFERENT ANATOMICAL LOCATIONS. MEDICAL ENGINEERING & PHYSICS 20(2): 124-131; 1998

163. RHO J-Y: AN ULTRASONIC METHOD FOR MEASURING THE ELASTIC PROPERTIES OF HUMAN TIBIAL CORTICAL AND CANCELLOUS BONE. ULTRASONICS 34(8): 777-783; 1996

164. REILLY DT, BURSTEIN AH: THE MECHANICAL PROPERTIES OF CORTICAL BONE. THE JOURNAL OF BONE & JOINT SURGERY 56(5): 1001-1022; 1974

165. GIBSON LJ: THE MECHANICAL BEHAVIOUR OF CANCELLOUS BONE. JOURNAL OF BIOMECHANICS 18(5): 317-328; 1985

166. TURNER CH, COWIN SC: DEPENDENCE OF ELASTIC CONSTANTS OF AN ANISOTROPIC POROUS MATERIAL UPON POROSITY AND FABRIC. JOURNAL OF MATERIALS SCIENCE 22(9): 3178-3184; 1987

167. COWIN SC, YANG G: AVERAGING ANISOTROPIC ELASTIC CONSTANT DATA. JOURNAL OF ELASTICITY 46(2): 151-180; 1997

168. PAHR DH, ZYSSET PK: INFLUENCE OF BOUNDARY CONDITIONS ON COMPUTED APPARENT ELASTIC PROPERTIES OF CANCELLOUS BONE. BIOMECHANICS AND MODELING IN MECHANOBIOLOGY 7(6): 463-476; 2008

169. BOUTROY S, VAN RIETBERGEN B, SORNAY-RENDU E, MUNOZ F, BOUXSEIN ML, DELMAS PD: FINITE ELEMENT ANALYSIS BASED ON IN VIVO HR-PQCT IMAGES OF THE DISTAL RADIUS IS ASSOCIATED WITH WRIST FRACTURE IN POSTMENOPAUSAL WOMEN. JOURNAL OF BONE AND MINERAL RESEARCH 23(3): 392-399; 2008

170. CHEVALIER Y, PAHR D, ALLMER H, CHARLEBOIS M, ZYSSET P: VALIDATION OF A VOXEL-BASED FE METHOD FOR PREDICTION OF THE UNIAXIAL APPARENT MODULUS OF HUMAN TRABECULAR BONE USING MACROSCOPIC MECHANICAL TESTS AND NANOINDENTATION. JOURNAL OF BIOMECHANICS 40(15): 3333-3340; 2007

171. WOLFRAM U, WILKE H-J, ZYSSET PK: VALID M FINITE ELEMENT MODELS OF VERTEBRAL TRABECULAR BONE CAN BE OBTAINED USING TISSUE PROPERTIES MEASURED WITH NANOINDENTATION UNDER WET CONDITIONS. JOURNAL OF BIOMECHANICS 43(9): 1731-1737; 2010

172. RODRIGUEZ-FLOREZ N, OYEN ML, SHEFELBINE SJ: INSIGHT INTO DIFFERENCES IN NANOINDENTATION PROPERTIES OF BONE. JOURNAL OF THE MECHANICAL BEHAVIOR OF BIOMEDICAL MATERIALS 18: 90-99; 2013

173. PANYASANTISUK J, PAHR DH, GROSS T, ZYSSET PK: COMPARISON OF MIXED AND KINEMATIC UNIFORM BOUNDARY CONDITIONS IN HOMOGENIZED ELASTICITY OF FEMORAL TRABECULAR BONE USING MICROFINITE ELEMENT ANALYSES. JOURNAL OF BIOMECHANICAL ENGINEERING 137(1): 011002; 2015

174. HAZANOV S: HILL CONDITION AND OVERALL PROPERTIES OF COMPOSITES. ARCHIVE OF APPLIED MECHANICS 68(6): 385-394; 1998

175. CIARELLI M, GOLDSTEIN S, KUHN J, CODY D, BROWN M: EVALUATION OF ORTHOGONAL MECHANICAL PROPERTIES AND DENSITY OF HUMAN TRABECULAR BONE FROM THE MAJOR METAPHYSEAL REGIONS WITH MATERIALS TESTING AND COMPUTED TOMOGRAPHY. JOURNAL OF ORTHOPAEDIC RESEARCH 9(5): 674-682; 1991

176. SCHILEO E, TADDEI F, MALANDRINO A, CRISTOFOLINI L, VICECONTI M: SUBJECT-SPECIFIC FINITE ELEMENT MODELS CAN ACCURATELY PREDICT STRAIN LEVELS IN LONG BONES. JOURNAL OF BIOMECHANICS 40(13): 2982-2989; 2007

177. KANEKO TS, BELL JS, PEJCIC MR, TEHRANZADEH J, KEYAK JH: MECHANICAL PROPERTIES, DENSITY AND QUANTITATIVE CT SCAN DATA OF TRABECULAR BONE WITH AND WITHOUT METASTASES. JOURNAL OF BIOMECHANICS 37(4): 523-530; 2004

178. KEYAK JH, FALKINSTEIN Y: COMPARISON OF IN SITU AND IN VITRO CT SCAN-BASED FINITE ELEMENT MODEL PREDICTIONS OF PROXIMAL FEMORAL FRACTURE LOAD. MEDICAL ENGINEERING & PHYSICS 25(9): 781-787; 2003

179. MINDWAYS: QCT PRO ™ - BONE MINERAL DENSITOMETRY SOFTWARE – CT CALIBRATION PHANTOM. FTP://193.42.153.91/QCT/EN/PHANTOM_EN.PDF (DATE OF ACCESS: AUGUST 18TH, 2016)

180. JANG KJ, CHOI JW, KWEON DC, LEE JW, GOO EH, DONG KR, LEE JS, JIN GH, SEO SB: MEASUREMENT OF IMAGE QUALITY IN CT IMAGES RECONSTRUCTED WITH DIFFERENT KERNELS. JOURNAL OF THE KOREAN PHYSICAL SOCIETY 58(2): 334-342; 2011

181. SITZER A: DETERMINATION AND VERIFICATION OF MATERIAL PROPERTIES RELATED TO CT DATA IN HUMAN CORTICAL BONE. MASTER THESIS. LÜBECK, 2010.

182. DREVER H: TRANSFORMING HUMAN FEMORAL BONE SAMPLES TO A REFERENCE SYSTEM ACCORDING TO PREDOMINANT TRABECULAR ORIENTATION. MASTER THESIS. LÜBECK, 2017.

183. KEYAK J, LEE I, SKINNER H: CORRELATIONS BETWEEN ORTHOGONAL MECHANICAL PROPERTIES AND DENSITY OF TRABECULAR BONE: USE OF DIFFERENT DENSITOMETRIC MEASURES. JOURNAL OF BIOMEDICAL MATERIALS RESEARCH PART A 28(11): 1329-1336; 1994

184. TAMMENA H: ENTWICKLUNG EINER MESSMETHODIK ZUR BESTIMMUNG VON SCHUBPARAMETERN HUMANER KNOCHENPRÄPARATE. DIPLOMA THESIS. LÜBECK, 2011.

185. DUBBEL H: DUBBELS TASCHENBUCH FÜR DEN MASCHINENBAU. 24TH EDITION, **C** 26-29, SPRINGER-VERLAG, BERLIN, HEIDELBERG, 2014

186. RIDLER T, CALVARD S: PICTURE THRESHOLDING USING AN ITERATIVE SELECTION METHOD. IEEE TRANSACTIONS ON SYSTEMS, MAN, AND CYBERNETICS 8(8): 630-632; 1978

187. ULRICH D, VAN RIETBERGEN B, WEINANS H, RÜEGSEGGER P: FINITE ELEMENT ANALYSIS OF TRABECULAR BONE STRUCTURE: A COMPARISON OF IMAGE-BASED MESHING TECHNIQUES. JOURNAL OF BIOMECHANICS 31(12): 1187-1192; 1998

188. HARRIGAN TP, JASTY M, MANN RW, HARRIS WH: LIMITATIONS OF THE CONTINUUM ASSUMPTION IN CANCELLOUS BONE. JOURNAL OF BIOMECHANICS 21(4): 269-275; 1988

189. ANDREWS E, GIOUX G, ONCK P, GIBSON L: SIZE EFFECTS IN DUCTILE CELLULAR SOLIDS. PART II: EXPERIMENTAL RESULTS. INTERNATIONAL JOURNAL OF MECHANICAL SCIENCES 43(3): 701-713; 2001

190. THOMPSON MS, MCCARTHY ID, LIDGREN L, RYD L: COMPRESSIVE AND SHEAR PROPERTIES OF COMMERCIALLY AVAILABLE POLYURETHANE FOAMS. JOURNAL OF BIOMECHANICAL ENGINEERING 125(5): 732-734; 2003

191. LANDEL RF, NIELSEN LE: MECHANICAL PROPERTIES OF POLYMERS AND COMPOSITES. 2ND EDITION, 33-36, CRC PRESS, BOCA RATON, 1993

192. BUZUG TM: COMPUTED TOMOGRAPHY: FROM PHOTON STATISTICS TO MODERN CONE-BEAM CT. 1ST EDITION, 28-432, SPRINGER SCIENCE & BUSINESS MEDIA, 2008

193. BROOKS RA, DI CHIRO G: BEAM HARDENING IN X-RAY RECONSTRUCTIVE TOMOGRAPHY. PHYSICS IN MEDICINE & BIOLOGY 21(3): 390; 1976

194. SUMNER D, OLSON C, FREEMAN P, LOBICK J, ANDRIACCHI T: COMPUTED TOMOGRAPHIC MEASUREMENT OF CORTICAL BONE GEOMETRY. JOURNAL OF BIOMECHANICS 22(6-7): 649-653; 1989

195. SITZER A, AULMANN L, WENDLANDT R, HANDELS H, WEYERS I, SCHULZ AP, BUZUG T: EVALUATION OF LOCAL ALTERATIONS IN FEMORAL BONE MINERAL DENSITY MEASURED VIA QUANTITATIVE CT. CURRENT DIRECTIONS IN BIOMEDICAL ENGINEERING 1(1): 327-330; 2015

196. LI B, ASPDEN RM: COMPOSITION AND MECHANICAL PROPERTIES OF CANCELLOUS BONE FROM THE FEMORAL HEAD OF PATIENTS WITH OSTEOPOROSIS OR OSTEOARTHRITIS. JOURNAL OF BONE AND MINERAL RESEARCH 12(4): 641-651; 1997

197. GIBSON LJ: THE MECHANICS OF THREE-DIMENSIONAL CELLULAR MATERIALS. PROCEEDINGS OF THE ROYAL SOCIETY OF LONDON SERIES A, MATHEMATICAL, PHYSICAL AND ENGINEERING SCIENCES 382(1782): 43-59; 1982

198. ABENDSCHEIN W, HYATT G: 33 ULTRASONICS AND SELECTED PHYSICAL PROPERTIES OF BONE. CLINICAL ORTHOPAEDICS AND RELATED RESEARCH 69: 294-301; 1970

199. NATALI A, MEROI E: A REVIEW OF THE BIOMECHANICAL PROPERTIES OF BONE AS A MATERIAL. JOURNAL OF BIOMEDICAL ENGINEERING 11(4): 266-276; 1989

200. LINDE F, NØRGAARD P, HVID I, ODGAARD A, SØBALLE K: MECHANICAL PROPERTIES OF TRABECULAR BONE. DEPENDENCY ON STRAIN RATE. JOURNAL OF BIOMECHANICS 24(9): 803-809; 1991

201. MÜLLER M: VALIDATION OF AN OPTICAL MEASUREMENT PROCEDURE FOR DETERMINATION OF ANISOTROPIC SHEAR PARAMETERS IN CANCELLOUS AND CORTICAL HUMAN FEMORAL BONE. MASTER THESIS. LÜBECK, 2014.

202. WENDLANDT R, SCHLITZKE M, SITZER A, SCHULZ AP: ORTHOTROPIC MATERIAL PARAMETERS OF SHORT-FIBER-FILLED EPOXY CYLINDERS AS ALTERNATIVE TEST MATERIAL FOR CORTICAL BONE. BIOMEDICAL ENGINEERING - BIOMEDIZINISCHE TECHNIK 59: S986-S986; 2014

203. BOURGNON A, SITZER A, CHABRABORTY A, ROHDE K, VARGA P, WENDLANDT R, RAUM K, EDITORS. IMPACT OF MICROSCALE PROPERTIES MEASURED BY 50-MHZ ACOUSTIC MICROSCOPY ON MESOSCALE ELASTIC AND ULTIMATE MECHANICAL CORTICAL BONE PROPERTIES. ULTRASONICS SYMPOSIUM (IUS), IEEE INTERNATIONAL; 2014.

204. LEE T, LAKES R: ANISOTROPIC POLYURETHANE FOAM WITH POISSON'SRATIO GREATER THAN 1. JOURNAL OF MATERIALS SCIENCE 32(9): 2397-2401; 1997

205. MADENCI E, GUVEN I: THE FINITE ELEMENT METHOD AND APPLICATIONS IN ENGINEERING USING ANSYS®. 2ND EDITION, 148-149, SPRINGER, NEW YORK, 2015

206. KABEL J, VAN RIETBERGEN B, DALSTRA M, ODGAARD A, HUISKES R: THE ROLE OF AN EFFECTIVE ISOTROPIC TISSUE MODULUS IN THE ELASTIC PROPERTIES OF CANCELLOUS BONE. JOURNAL OF BIOMECHANICS 32(7): 673-680; 1999

207. RHO J-Y, KUHN-SPEARING L, ZIOUPOS P: MECHANICAL PROPERTIES AND THE HIERARCHICAL STRUCTURE OF BONE. MEDICAL ENGINEERING & PHYSICS 20(2): 92-102; 1998

208. HOBATHO MC, RHO JY, ASHMAN RB: ANATOMICAL VARIATION OF HUMAN CANCELLOUS BONE MECHANICAL PROPERTIES IN VITRO. IN: LOWET G, RÜEGSEGGER P, WEINANS H, MEUNIER A: BONE RESEARCH IN BIOMECHANICS. 40, 157-173, IOS PRESS., AMSTERDAM, 1997

209. WOLFRAM U, WILKE H-J, ZYSSET PK: REHYDRATION OF VERTEBRAL TRABECULAR BONE: INFLUENCES ON ITS ANISOTROPY, ITS STIFFNESS AND THE INDENTATION WORK WITH A VIEW TO AGE, GENDER AND VERTEBRAL LEVEL. BONE 46(2): 348-354; 2010

210. CHEN X, LAM Y: CT DETERMINATION OF THE MINERAL DENSITY OF DRY BONE SPECIMENS USING THE DIPOTASSIUM PHOSPHATE PHANTOM. AMERICAN JOURNAL OF PHYSICAL ANTHROPOLOGY 103(4): 557-560; 1997

211. SCHENZLE JC, SOMMER WH, NEUMAIER K, MICHALSKI G, LECHEL U, NIKOLAOU K, BECKER CR, REISER MF, JOHNSON TR: DUAL ENERGY CT OF THE CHEST: HOW ABOUT THE DOSE? INVESTIGATIVE RADIOLOGY 45(6): 347-353; 2010

212. AULMANN LF: UNTERSUCHUNG VON MESSUNGENAUIGKEITEN MITTELS QUANTITATIVER COMPUTERTOMOGRAPHIE BESTIMMTER KNOCHENMINERALDICHTE HUMANER FEMORA. BACHELOR THESIS. LÜBECK, 2011.

213. MARTIN RB: DETERMINANTS OF THE MECHANICAL PROPERTIES OF BONES. JOURNAL OF BIOMECHANICS 24: 79-88; 1991

214. ENGELKE K, ADAMS JE, ARMBRECHT G, AUGAT P, BOGADO CE, BOUXSEIN ML, FELSENBERG D, ITO M, PREVRHAL S, HANS DB: CLINICAL USE OF QUANTITATIVE COMPUTED TOMOGRAPHY AND PERIPHERAL QUANTITATIVE COMPUTED TOMOGRAPHY IN THE MANAGEMENT OF OSTEOPOROSIS IN ADULTS: THE 2007 ISCD OFFICIAL POSITIONS. JOURNAL OF CLINICAL DENSITOMETRY 11(1): 123-162; 2008

215. SAVVIDIS E, LÖER F, GRÜTERS H, WIESENER C: ANALYSE DER BEANSPRUCHUNG DES PROXIMALEN FEMUR BEI VERSCHIEDENEN ARTEN DER BELASTUNG MIT HILFE DER FINITE-ELEMENT-METHODE. ZEITSCHRIFT FÜR ORTHOPÄDIE UND IHRE GRENZGEBIETE 129(03): 268-277; 1991

216. RÖHRLE H, SCHOLTEN R, SOLLBACH W, RITTER G, GRÜNERT A: DER KRAFTFLUß BEI HÜFTENDOPROTHESEN. ARCHIVES OF ORTHOPAEDIC AND TRAUMA SURGERY 89(1): 49-60; 1977

217. WHITEHOUSE W, DYSON E: SCANNING ELECTRON MICROSCOPE STUDIES OF TRABECULAR BONE IN THE PROXIMAL END OF THE HUMAN FEMUR. JOURNAL OF ANATOMY 118(PT 3): 417; 1974

218. MULDER L, VAN RIETBERGEN B, NOORDHOEK NJ, ITO K: DETERMINATION OF VERTEBRAL AND FEMORAL TRABECULAR MORPHOLOGY AND STIFFNESS USING A FLAT-PANEL C-ARM-BASED CT APPROACH. BONE 50(1): 200-208; 2012

ACKNOWLEDGEMENTS

First, I would like to thank my great supervisor Professor Arndt Peter Schulz for his scientific advice, his trust and his open-hearted way to lead people. It was very motivating and with the end of this thesis, I'll lose a bit of a family. My deepest gratitude also goes to my advisor Dr. Ing. Robert Wendlandt for his excellent scientific, technical and statistical support. Your smart approaches were really inspiring.

Moreover, I would like to thank Dr. med. Imke Weyers, Nadine Teletzky and all other helping hands of the Institute of Anatomy, University of Lübeck, who supported this work by the provision of cadaveric material and their excellent dissection skills. In this context, it would be remiss of me not to thank all body donors of this study post mortem. Without their contribution this work would not have been possible.

I am also grateful for the support of Professor Buzug, Jan, Maren, Sylvia and Aileen of the Institute of Medical Engineering, University of Lübeck, who contributed to this work with their skills in computed tomography. The same applies to Professor Botterweck and his team from the Laboratory of Medical Imaging, University of Applied Sciences Lübeck, who contributed to the acquisition of micro computed tomographic images. In this context, I am especially grateful for the support of Tobias. Your door was always open to me and it was a real pleasure to work with you.

I would furthermore like to thank Andreas Petersik and the entire team of Stryker Trauma GmbH for their great support and the registration of femora on their statistical model. I also want to thank Uwe Wolfram and Dieter Pahr for their valuable advice on micro finite element analysis of bone.

I would like to give very special thanks to Klaus. You were my good soul over all the past years and your assistance in milling, testing and embedding was of greatest value. I would like to thank Lina for the support in bone handling and testing. I am also grateful for the valuable exchange of knowledge with Tanja and Gereon. It was a pleasure to have such amazing bone-companions. I especially want to thank all my hardworking students. Your work was more than helpful and I

like to remember all the fun times we've had. In particular, I would like to thank Hauke for the design of the torsion machine, Linda for the support in the QCT assessment study, Matthias for the introduction into morphological investigations, Marcus for the support in torsional measurements of PU foam, Matthias for the valuable support in MATLAB, Alex for the mechanical testing of PU-samples and Henning for the excellent job in image registration, image processing, segmentation of trabecular samples, the determination of sample grey values and trabecular eigensystems as well as the preparation of μFEA. Unless mentioned before, I would also like to thank all co-authors for their contribution to our manuscripts.

My deepest gratitude goes to my beloved friends and my family, who supported me during the hard times. As you can see Mum, the New Kids on the Block VHS tape was really worth the money. I would also like to thank my sweet little son Jonah Nicolae for his patience with his mum working on this doctoral thesis. In this context, I want to thank Regina and Nico for their hospitality. You are truly amazing babysitters.

In the end, I would like to thank the most significant person in my life: my wonderful husband Florian. I really appreciate your outstanding support through our studies and this doctoral thesis. I cannot emphasize strongly enough, how you inspire(d) me every single day with all your skills, your technical and scientific advice, your emotional support and your love.

INDEX